Spring 5-2016

Progress towards Bose-Einstein condensation on an atom chip as a functional testbed for experiments aboard the orbital NASA Cold Atom Laboratory

Daniel Adkins Paseltiner
Bates College, dpaselti@bates.edu

Progress towards Bose-Einstein condensation on an atom chip as a functional testbed for experiments aboard the orbital NASA Cold Atom Laboratory

Daniel Paseltiner

DEPARTMENT OF PHYSICS AND ASTRONOMY, BATES COLLEGE, LEWISTON, ME 04240

Progress towards Bose-Einstein Condensation on an atom chip as a functional testbed for experiments aboard the orbital NASA Cold Atom Laboratory

Daniel Paseltiner

Advisor: Nathan Lundblad

An Honors Thesis

Presented to the Department of Physics and Astronomy

Bates College

in partial fulfillment of the requirements for the

Degree of Bachelor of Science

Lewiston, Maine

March 28, 2016

Contents

Acknowledgments

I would not have been able to write this thesis without the help and support of many people. Although I cannot mention them all, there are few people that I would like to thank. To begin, I must start with my family Mom, Dad, Matthew, and Isaac. You have always been there to support me by providing the right balance of empathy and pressure to encourage me along. I am forever grateful to you for all of your care and love.

Beginning with my primary education and extending through my time at Bates I have had the great fortune of being taught by many terrific teachers. Earlier this year I came to the realization that my introduction to Atomic, Molecular and Optical physics came when I was in fourth and fifth grade learning about basic atomic structure, the Periodic table, and building molecular models. Now here I am ten years later having completed this thesis working in a BEC lab. Kathy Allen and Gerry Leonard, thank you for starting me down this path. The lessons I learned with you continue prove their great worth both inside and outside academia.

Frank Aulenti, your enthusiasm and love of science certainly rubbed off in eighth grade. Thank you for encouraging the same in me. The hours you spent teaching me how to solder after school have served me well on many occasions, especially when building the electronics we will discuss in Ch. 5.

Kristen Amon, in a stricter sense my introduction to physics was junior year of high school in your honors physics class, which morphed in A.P. Physics a year later. When I think back on my time at Stamford High some of the first memories that come to mind are of being in your classroom. To this day I remember the kinematics equations by their color and location on your wall. Thank you for tolerating our shenanigans for two years and the wonderful introduction to physics.

I will always be indebted to the faculty of the physics department at Bates for their instruction, support, care, and commitment. Prof. Mark Semon, because of you I appreciate that it is better to uncover a little than to cover a lot and that there is always time for a "liberal arts moment". Prof. Eric Wollman, although I only had the pleasure of taking one course with you, it was the first time I felt like I was learning to think like a physicist. Prof. Travis Gould, after five courses your insightful instruction has formed a cornerstone of my time at Bates, thank you. Prof. Hong Lin, the last two semesters of quantum mechanics have been intriguing and indispensable in writing this thesis, thank you. Dr. Tom Jarvis, your patience and tutelage in lab have been a true gift. Thank you for the many enjoyable and instructive hours aligning optics and locking the repump laser.

Last but emphatically not least, Prof. Nathan Lundblad. Taking Lab Physics with you sophomore year, convinced me to pursue physics at a graduate level. From our first meeting when I left your office with my head spinning trying comprehend how in the world lasers could actually cool atoms, to our most recent discussions about the time evolution of the density matrix, your mentorship has been invaluable. Thank you for agreeing to work with me on this project, and giving me the opportunity to be apart of your research. It has been a challenging, yet rewarding experience.

Introduction

In 1924 Satyendra Nath Bose sent a manuscript to Einstein, in which he presented a statistical study of Planck's black body spectrum. Einstein translated the paper into German and published it later that year [1]. Then in 1925 Einstein published a second paper on the topic [2] generalizing Bose's approach to an ideal Bose gas. These two papers introduced for the first time, what we now know as Bose-Einstein statistics. As we will see in Ch. 1, this theory predicts that when a system of bosons, particles that do not obey the Pauli exclusion principle, is sufficiently cold and dense large portions of the system's population will enter or condense into the ground state forming a Bose-Einstein Condensate (BEC). The development of the laser cooling, magneto-optical trapping, magnetic trapping, and radiofrequency evaporation in the 1970's and 80's eventually allowed Cornell and Wieman at Boulder, Ketterle at MIT, and Hulet at Rice to observe the first BECs in 1995 [3, 4, 5]. In recognition of the their work Cornell, Wieman, and Ketterle were awarded the Nobel Prize in Physics in 2001 [6, 7]. Since their initial production the study of BECs has offered exciting new insights into many fields including quantum mechanics and solid state physics [8].

As research with BECs has continued further progress in certain areas has been stunted due to a ubiquitous challenge, gravity. It is possible to experimentally negate the effects of the Earth's magnetic field but there is no recourse for handling its gravitational field. One way to study BECs in absence of gravitational effects is to place them in free fall, thereby creating a microgravity environment, which can be accomplished in one of two ways. One method for doing this is to simply drop an entire BEC experiment from a great height and observe the condensates it produces as it falls, which was first done in 2010 [9]. This method has the downside of the placing a restriction on the duration of the experiment because the amount of the time in free fall is finite. Alternatively, a BEC experiment could be put into orbit around the Earth. This is precisely what the NASA Cold Atom Laboratory project (CAL) aims to do by installing a BEC experiment aboard the International Space Station (ISS). For a long time the size and high power consumption of BEC experiments would have made operating one on the ISS an insurmountable challenge. However, the development of magnetic trapping on atom chips, non-conducting surfaces with conducting lithographic traces printed on them, make such an endeavor possible, due to their decreased power consumption, and small form factor.

This thesis presents the development of an atom chip based BEC experiment similar to CAL at Bates College, that will serve as a functional testbed for future research aboard the ISS. Both a theoretical background and a description of the experimental process by which a BEC is formed on the atom chip are provided. This process is primarily driven by laser cooling and magnetic trapping techniques. A 2D+ Magneto-Optical Trap (MOT), loaded from vapor pressure, is used as a slowed source of ^{87}Rb in order to load a 3D MOT. We present a qualitative description of the 2D MOT, a discussion several experimental challenges encountered over the course of the semester, and outline a path forward to condensation in a chip-based magnetic trap through the use of radiofrequency evaporative cooling. To accomplish these goals this thesis is structured around answering the following three questions:

(1) What is a BEC?

(2) What techniques can we use to make a BEC?

(3) How can we implement these techniques experimentally?

Question 1 is answered in Ch. 1 where the process of Bose-Einstein condensation is described starting with a derivation of the relevant statistical mechanics and distribution functions. This chapter ends by generalizing the conditions for condensation to an arbitrary confining potential and introducing the Thomas-Fermi approximation. Before moving on to question 2, Ch. 2 provides a discussion of the semi-classical description of atom-light interactions. This is done by deriving the Optical Bloch equations, with the goal of developing an expression for the scattering rate of an atom in a near resonant radiation field. Relying on the results of the previous chapter, Ch. 3 provides the first part of the answer to question 2 with a theoretical description of laser cooling and magneto-optical trapping. The answer to question 2 is completed in Ch. 4 where magnetic trapping and radiofrequency evaporation are described. This chapter focuses on the use of straight conductors to form magnetic traps specifically those that might be formed on an atom chip. Question 3 is then answered in Ch. 5 which provides a detailed description of the experimental systems we have built over the last two semesters and how they will be used to achieve Bose-Einstein condensation. Finally, Ch. 6 provides a discussion of the progress made this semester, current standing, and outlook for the experiment at Bates and the CAL project at large.

Bose-Einstein Condensation

In this chapter we will develop a theory to describe Bose-Einstein condensation and the resulting BECs. To do this we will start by considering the quantum mechanical behavior of indistinguishable particles. Since we are ultimately interested in considering ensembles of large numbers, a purely quantum mechanical description will prove to be impractical and a statistical approach will be required. We derive the basics of Boltzmann statistics and quantum statistics and use the resulting distribution functions to see that in the proper conditions BEC should form.

1. Bosons and Fermions

In this section we will start by considering a system of two distinguishable particles and progress to the indistinguishable case following the derivation in [**10**]. Assume that these particles are in states $\Psi_a(\mathbf{r}_1)$, and $\Psi_b(\mathbf{r}_2)$ respectively, neglecting spin. In this case $\Psi(\mathbf{r}_1, \mathbf{r}_2)$, ignoring the possibility of entangled states, can be written as

$$(1.1) \qquad \Psi(\mathbf{r}_1, \mathbf{r}_2) = \Psi_a(\mathbf{r}_1)\Psi_b(\mathbf{r}_2).$$

Our assumption of distinguishable particles is implicit in this statement because it requires us to be able to definitively say that particle 1 is in state Ψ_a, and particle 2 is in state Ψ_b. From a classical stand point this seems like an absurd concern, since we should be able to somehow label or mark the particles to clearly distinguish them. However, if our system comprises two particles of the same species, say two electrons, or as will be our case in lab, two ^{87}Rb atoms because these particles are completely identical, and we have no way of labeling them, so they are indistinguishable. As Griffiths says "It is not just that we don't happen to know which electron is which; God doesn't know which is which, because there is no such things as this electron or that electron."

To accommodate the case of indistinguishable particles we can rewrite equation 1.1 as

$$(1.2) \qquad \Psi_\pm(\mathbf{r}_1, \mathbf{r}_2) = A[\Psi_a(\mathbf{r}_1)\Psi_b(\mathbf{r}_2) \pm \Psi_b(\mathbf{r}_1)\Psi_a(\mathbf{r}_2)],$$

where A is a constant of normalization. This allows us to deal with our uncertainty as to which particle is in which state by taking advantage of a linear combination in which either the two states we are using as a basis, $\Psi_a(\mathbf{r}_1)\Psi_b(\mathbf{r}_2)$ and $\Psi_b(\mathbf{r}_1)\Psi_a(\mathbf{r}_2)$, have the same or opposite signs. This indicates the existence of two kinds of indistinguishable particles, bosons for which the possible states add, and fermions for which the possible states subtract. To show the difference between how fermions and bosons behave we will consider the case in which both particles are in the same state, $\Psi_a = \Psi_b$. Applying this condition to the two equations represented in 1.2 results in

$$(1.3) \qquad \Psi_-(\mathbf{r}_1, \mathbf{r}_2) = A[\Psi_a(\mathbf{r}_1)\Psi_a(\mathbf{r}_2) - \Psi_a(\mathbf{r}_1)\Psi_a(\mathbf{r}_2)] = 0,$$

and

(1.4) $$\Psi_+(\mathbf{r}_1, \mathbf{r}_2) = A[\Psi_a(\mathbf{r}_1)\Psi_a(\mathbf{r}_2) + \Psi_a(\mathbf{r}_1)\Psi_a(\mathbf{r}_2)] = 2A\Psi_a(\mathbf{r}_1)\Psi_a(\mathbf{r}_2).$$

In this case $\Psi_- = 0$ which means that is no chance of finding two fermions same state. This fundamental property of fermions is known as the Pauli exclusion principle. On the other hand $\Psi_+ \neq 0$ which shows that this restriction does not apply to bosons. It is precisely the fact that there is no restriction on the number of bosons in a given state that allows for them to form a BEC! This property of bosons will be the object of our further study.

Using equation 1.4 as a mode we can write Ψ_+ for a system of N bosons in the same state, if we lump all of the constants into A, as:

(1.5) $$\Psi_+ = A \prod_{n=1}^{N} \Psi_a(\mathbf{r}_n).$$

Unfortunately we have now run into the impracticality of this method for treating indistinguishable particles. It is true that thus far the equations have been manageable, but we have only considered a system consisting of 2 particles. There are N terms in the product on the RHS of equation 1.5 for a system of N particles. We are interested in studying systems with numbers of particles on the order of at least 10^5 and there is not space in this entire thesis for 10^5 terms. To describe systems of a large number of indistinguishable particles, and ultimately the phenomenon of Bose-Einstein Condensation, we will need to apply the insight gained from this brief foray into quantum mechanics to a statistical approach, which is the topic of the next section.

2. Statistical Mechanics

As we saw in the previous section it would futile to attempt to describe an ensemble of indistinguishable particles by explicitly considering each particle's wavefunction. Fortunately, statistical mechanics provides us with a powerful tool that will allow us to move forward. We will now develop statements for the probability of a particle occupying a given state. We will do this first for particles in the high temperature limit by developing what are known as Boltzmann statistics. While not our ultimate goal Boltzmann statistics offers a good description of particles before condensation, which will be useful when describing evaporative cooling later on. They also provide a good point of comparison for the descriptions we will develop for fermions and bosons that are accurate outside the high temperature limit. The work in this section loosely follows [**11**], although similar derivations can be found in almost any introductory statistical mechanics text.

2.1. Boltzmann Statistics. To begin we will consider a system, with some energy E, in thermal equilibrium with a significantly larger reservoir with energy U_R at a well defined temperature T. We will allow the system and reservoir to exchange energy, but not particles. Let's say that the system is in a state s_1 with energy $E(s_1)$ and the probability of being in this state is $P(s_1)$. Together the system and the reservoir form an isolated system, which means that all microstates are equally probable. When the system is in s_1 the reservoir will have some number of accessible microsates: this number is known as its multiplicity and I will denote it by $\Omega_R(s_1)$. As $E(s_1)$ increases $\Omega_R(s_1)$ will decrease because the system will have less energy causing it to have a smaller number of accessible microstates, which means that $P(s_1)$ will decrease.

The converse is of course true if $E(s_1)$ decreases. We can conclude that $P(s_1)$ is proportional to $\Omega_R(s_1)$, which allows us to write that

$$(1.6) \qquad P(s_1) = \alpha\Omega_R(s_1),$$

where α is some as yet unknown constant of proportionality. To eliminate α we will consider the ratio between $P(s_2)$ and $P(s_2)$

$$(1.7) \qquad \frac{P(s_2)}{P(s_1)} = \frac{\Omega_R(s_2)}{\Omega_R(s_1)},$$

where s_2 is some second state of the system. We will now take advantage of the definition of entropy that $S = k\ln(\Omega)$ to rewrite Ω_R:

$$(1.8) \qquad \frac{P(s_2)}{P(s_1)} = \frac{e^{S_R(s_2)/k}}{e^{S_R(s_1)/k}} = e^{[S_R(s_2)-S_R(s_1)]/k}.$$

Now we need to consider that systems change in entropy from s_1 to s_2. Since the system is small as compared to the reservoir we can make use of the thermodynamic identity:

$$(1.9) \qquad dS_R = \frac{1}{T}(dU_R + PdV_R - \mu dN_R).$$

In practice $PdV_R \ll dU_R$ so we will take the contribution of PdV_R to be negligible and drop the term. Additionally, we are not allowing particles to enter or leave the system, therefore $\mu dN_R = 0$. Now keeping in mind that whatever energy the reservoir gains the system must lose, the change in entropy in equation 1.8 can be written as

$$(1.10) \qquad S_R(s_2) - S_R(s_1) = \frac{1}{T}[U_R(s_2) - U_R(s_1)] = -\frac{1}{T}[E(s_2) - E(s_1)].$$

Plugging into equation 1.8 yields,

$$(1.11) \qquad \frac{P(s_2)}{P(s_1)} = e^{-[E(s_2)-E(s_1)]/kT} = \frac{e^{-E(s_2)/kT}}{e^{-E(s_1)/kT}}$$

Each of the exponential factors is know as a Boltzmann factor.

To learn more from equation 1.11 we need to rearrange it so that all s_1 dependence is one side and the s_2 dependence is on the other, which results in

$$(1.12) \qquad \frac{P(s_2)}{e^{-E(s_2)/kT}} = \frac{P(s_1)}{e^{-E(s_1)/kT}} = \alpha$$

It is now easy to see that since both sides are completely independent of each they must be constant, which if we go back and check equation 1.6 must be α which means that it can generalized to:

$$(1.13) \qquad P(s) = \alpha\Omega_R(s) = \alpha e^{-E(s)/kT}.$$

We now have enough information to find an expression for α. Since the particle must be in a state some over the probabilities of being in each state must be one which means that:

$$(1.14) \qquad \sum_s P(s) = \alpha \sum_s e^{-E(s)/kT} = 1.$$

Most authors define this constant α to be $1/Z$ to end up with the final equations:

$$(1.15) \qquad P(s) = \frac{1}{Z} e^{-E(s)/kT},$$

and

$$(1.16) \qquad Z = \sum_s e^{-E(s)/kT}.$$

Equation 1.16 is the so called partition function and in conjunction with 1.15 is the workhorse of statistical mechanics. However, we are rarely interested in considering a system of just one particle. Generalizing our the results of this section to a system of many particles in our next challenge.

2.2. The Maxwell-Boltzmann Distribution. We are now going expand on equations 1.15 and 1.16 to consider a system of N particles. Instead of considering the probability of a particle being in a given state we will consider the average number of particles in a given state, also known as the occupancy of state. This will be denoted as $\bar{n}_{MB}$, where the MB stands for Maxwell-Boltzmann to avoid confusion when we develop different expressions for occupancy when consider fermions and bosons specifically in later sections.

The probability of a being in a state can also be thought of as the fraction of the total number of particles that will occupy that state on average and so we can write that

$$(1.17) \qquad \bar{n}_{MB} = NP(s) = \frac{N}{Z_1} e^{-E(s)/kT},$$

where Z_1 is the partition function for a single particle in the system. Since Z_1 represents that possible states of one particle it makes sense to that that Z, the partition function for the entire system, can be written as

$$(1.18) \qquad Z = \frac{1}{N!} Z_1^N.$$

The $N!$ term must be introduced to correct our counting since we are dealing with indistinguishable particles. Combining this statement for Z along with the following two results, from a further study in Boltzmann statistics

$$(1.19) \qquad F = -kT \ln Z, \text{ and } \mu = \left(\frac{\partial F}{\partial N} \right)_{T,V},$$

where F is Helmholtz energy, we can write that:

$$(1.20) \qquad \mu = -kt \ln(Z_1/N).$$

Finally, plugging back into equation 1.18 and simplifying we find that:

(1.21)
$$\bar{n}_{MB} = e^{-[E(s)-\mu]/kT}.$$

This result is known as the Maxwell-Boltzmann distribution, and as we said earlier provides an expression for the occupancy of state as a function of its energy and temperature of the system.

Although I did not specifically mention this at the time, we made a significant assumption in equation 1.18. This statement assumes that no two particles will "want" to be in the same state, or to avoid the anthropomorphism, that the number of the single particle states is much greater than the number of particles which can be represented by the condition that

(1.22)
$$Z_1 \gg N.$$

This assumption was also embedded into the derivation when we took the μdn term in equation 1.9 to be zero. In the high temperature limit this condition is met because distance between particles is large as compared to their matter waves, as in the case of an ideal gas. If we are going to move forward thinking in terms of temperature it would be nice for this condition to have an explicit temperature dependence. This can be accomplished by introducing the thermal de Broglie wavelength, $\lambda_{th} = h/\sqrt{2\pi mkT}$, which is almost the true de Broglie wavelength, $\lambda = h/p$ and is frequently used in statistical mechanics, to quantify the realistic range of a particle's probability distribution in one dimension. The cube of the thermal de Broglie wavelength, λ_{th}^3 gives the volume in which it is probable to find a particle, this is known as a particle's quantum volume. We can now rephrase equation 1.22 as

(1.23)
$$\frac{V}{N} \gg \left(\frac{h}{\sqrt{2\pi mkT}} \right)^3.$$

This is known as the thermodynamic limit.

So, Boltzmann statistics are only valid when the volume per particle is much greater than the quantum volume of a particle in the system. By increasing temperature and/or decreasing temperature sufficiently we should be able to violate this condition, in which case quantum effects will begin to come into play. This is precisely what we are interested in, if we are going to further investigate bosons' freedom to have any number of particles in a state! We must now modify our statistical approach to allow for more than one particle to be in one state, this is the case considered in Quantum Statistics.

2.3. Quantum Statistics. We will now revisit our reservoir and system model that served as the basis for developing Boltzmann statistics, but with one catch. Now we will permit the reservoir and system to exchange particles in addition to energy.

We will proceed in the same manner as before and nothing will change in our derivation until we reach the equivalent of equation (1.8), and need to invoke the thermodynamic identity. At this point we will still take PdV to be zero, but since particles are now allowed to be exchanged clearly μdN is in general not zero, so we must keep this term. This leads us to:

(1.24)
$$\frac{P(s_2)}{P(s_1)} = e^{-[E(s_2)-E(s_1)-\mu N(s_2)+\mu N(s_1)]/kT} = \frac{e^{-[E(s_2)-\mu N(s_2)]/kT}}{e^{-[E(s_1)-\mu N(s_1)]/kT}},$$

instead of equation (1.9). Again we will proceed just as before only this time we will call the constant of proportionality $1/\mathcal{Z}$ and find that:

$$(1.25) \qquad P(s) = \frac{1}{\mathcal{Z}} e^{-[E(s)-\mu N(s)]/kT},$$

and

$$(1.26) \qquad \mathcal{Z} = \sum_s e^{-[E(s)-\mu N(s)]/kT}.$$

These two equations are analogous to equations 1.15, and 1.16, and $\mathcal{Z}$ is the so called grand partition function. The real difference in this approach comes in clear in our next step, which will be to use the grand partition function to find a distribution function for a system, because we must treat fermions and bosons separately.

Until now we have conceptualized our system as containing particles and made statements about the probability of a particle occupying a give state. We will now change our point of view and consider a system state and make statements about the probability of it being occupied by a number of particles. Let's say that this state is occupied by n particles, has a chemical potential μ, and each particle in this state has an energy ϵ. The probability of this state being occupied by n particles is

$$(1.27) \qquad P(n) = \frac{1}{\mathcal{Z}} e^{-n(\epsilon-\mu)/kT},$$

the product of each particle's individual probability of being in the state. To move on we will need an expression for the grand partition function, but to do this requires choosing whether we care considering fermions or bosons. Finally, quantum mechanics enters the picture! Let's begin with fermions.

2.4. The Fermi-Dirac Distribution. As we know fermions obey the Pauli exclusion principle which means that n can only be 0 or 1. So the grand partition function for a system of fermions is

$$(1.28) \qquad \mathcal{Z} = \sum_{n=0}^{1} e^{-n(\epsilon-\mu)/kT} = 1 + e^{-(\epsilon-\mu)/kT}.$$

just as we reasoned earlier the occupancy, which I will now call $\bar{n}_{FD}$ for Fermi-Dirac, can be written as:

$$(1.29) \qquad \bar{n}_{FD} = \sum_{n=0}^{1} nP(n) = P(1).$$

From here it is quite simple to use the results in equations 1.27 and 1.28 to get an expression for $P(1)$, after simplifying we find that:

$$(1.30) \qquad \bar{n}_{FD} = \frac{1}{e^{(\epsilon-\mu)/kT} + 1}.$$

This result is called the Fermi-Dirac distribution.

2.5. The Bose-Einstein Distribution. Now we will follow a similar procedure for a system of bosons, which we have shown do not obey the Pauli exclusion principle. This means that in principle that grand partition function for a system of bosons is the infinite series,

$$(1.31) \qquad \mathcal{Z} = 1 + e^{-(\epsilon-\mu)/kT} + e^{-2(\epsilon-\mu)/kT} + e^{-3(\epsilon-\mu)/kT} + \dots.$$

Fortunately this is a geometric series with a common ratio between terms of $e^{-(\epsilon-\mu)/kT} < 1$, because $\epsilon < \mu$, since the Gibbs factors cannot keep growing without limit. Therefore, the series must converge, and we can write that:

$$(1.32) \qquad \mathcal{Z} = \frac{1}{1 - e^{-(\epsilon-\mu)/kT}}.$$

Now, with $\mathcal{Z}$ in hand we can write the occupancy, now $\bar{n}_{BE}$ for Bose-Einstein, as before:

$$(1.33) \qquad \bar{n}_{BE} = \sum_n nP(n) = \sum_n n\frac{1}{\mathcal{Z}}e^{-n(\epsilon-\mu)/kT}.$$

We have now run into another potentially infinite sum. To handle this one we will play a small trick with some calculus, and make the the notation tidier by letting $x = (\epsilon-\mu)/kT$. Continuing from equation 1.33,

$$
\begin{aligned}
\sum_n n\frac{1}{\mathcal{Z}}e^{-n(\epsilon-\mu)/kT} &= \frac{1}{\mathcal{Z}}\sum_n ne^{-nx} \\
&= -\frac{1}{\mathcal{Z}}\sum_n \frac{\partial}{\partial x}e^{-nx} \\
(1.34) \qquad &= -\frac{1}{\mathcal{Z}}\frac{\partial \mathcal{Z}}{\partial x}.
\end{aligned}
$$

Now all that is left to do is to integrate, and simply. So, sparring the reader the intermediate calculus and and algebra we find that:

$$(1.35) \qquad \bar{n}_{BE} = \frac{1}{e^{(\epsilon-\mu)/kT} - 1}.$$

This is the so called Bose-Einstein distribution and describes the occupancy of a given state of a system of bosons. In the next section we will use it to describe Bose-Einstein condensation by investigating its behavior. To motivate this exercise I would first like to first compare the three distribution functions developed in this section, Maxwell-Boltzmann, Fermi-Dirac, and Bose-Einstein, as shown in Figure 1.1.

As we should hope states with high energy or when $(\epsilon-\mu)/kT \gg 1$ all three distributions predict the same occupancy. However, things become more interesting in state with lower energy. Since, we did not consider quantum effects in our derivation for the Maxwell-Boltzmann distribution, and we are now in the regime where they should play a role, it is fair to say that it will not give an accurate prediction of occupancy. So discounting the Maxwell-Boltzmann distribution we are left with the Fermi-Dirac, and Bose-Einstein distributions, which display remarkably different behavior. As ϵ decreases for a given system state more particles will have access to it. Since, only one fermion may occupy a given state and a given time it is reasonable that the Fermi-Dirac distribution approaches 1. On the other hand, because bosons do not
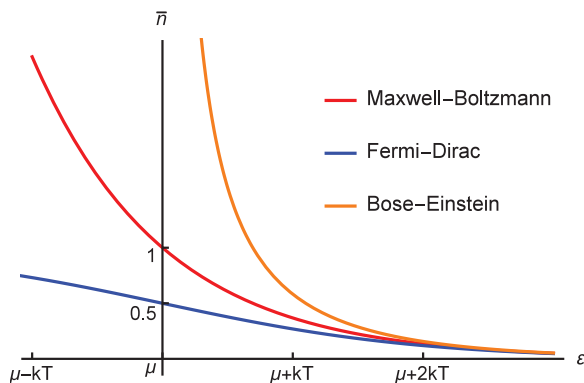
FIGURE 1.1. A comparison of the Maxwell-Boltzmann, Fermi-Dirac, and Bose-Einstein distributions for a fixed T and μ.

have this restriction the Bose-Einstein distribution blows up. This behavior suggests two questions: first, what happens when there is a large number of bosons in a state, and second, is there a way to force many bosons to occupy the same state? The answers to these questions will the topic of the next section.

3. Bose-Einstein Condensation

In this section we will return to the Bose-Einstein distribution to describe the process of Bose-Einstein condensation. This derivation has been compiled from those presented in [**11, 12, 13, 14, 15, 16**]. To begin let's consider a system of N non-interacting bosons in the low temperature limit, $T \to 0$. In this case the vast majority of the energy has been removed from the system and a particle must reside in the lowest-energy available state. For bosons this will always be the ground state with energy ϵ_0 so they must all occupy the ground state. This is to say that:

$$(1.36) \qquad \lim_{T \to 0} \frac{1}{e^{(\epsilon_0 - \mu)/kT} - 1} = N$$

Of course mathematically the Bose-Einstein distribution approaches infinity in this case, but this is clearly not a physical result as it would violate the conservation of mass. So the reasonable interpretation of this limit is that as temperature decreases the occupancy of the ground state will increase until, when it is cold enough, it becomes N. This suggests some sort of condensation process, although as we will see later it is not necessary to reach absolute zero for there to be large number of atoms in the ground state.

We will now consider two groups of particles in this system, particles in the ground state with an occupancy of N_0, and particles in all the excited states($\epsilon \neq \epsilon_0$) with an occupancy of N_e, so that $N = N_0 + N_e$. From the Bose-Einstein distribution we know that:

$$(1.37) \qquad N_0 = \frac{1}{e^{(\epsilon_0 - \mu)/kT} - 1},$$

and

$$(1.38) \qquad N_e = \sum_{\text{all } s} \frac{1}{z^{-1}e^{\epsilon_s/kT} - 1},$$

where I have let $z = e^{\mu/kT}$, which is known as the fugacity. To make further analytic progress we will need to convert the summation to an integral. To do this more easily we will introduce the density of states $a(\epsilon)$, the number of single particle states per unit energy. For some volume V with particles of mass m,

$$(1.39) \qquad a(\epsilon) = \frac{2}{\sqrt{\pi}} \left(\frac{2\pi m}{h^2} \right)^{3/2} V \sqrt{\epsilon}.$$

It is important to realize that the $a(\epsilon)$ gives a zero weight to the ground state $\epsilon_0 = 0$. Normally, in the thermodynamic limit we don't worry about this because so few particles will be in the ground state that dropping them from the total will have a negligible effect. In our case, however, we know that that $N_0 \gg 0$, so dropping it would have a significant impact. To correct for this we will use equation 1.37 to add N_0 back in explicitly. Now rewriting the summation as an integral:

$$
\begin{aligned}
N &= N_e + N_0 \\
&= \int_0^\infty a(\epsilon) \frac{1}{z^{-1} e^{\epsilon/kT} - 1} d\epsilon + N_0 \\
(1.40) \qquad &= \frac{2}{\sqrt{\pi}} \left(\frac{2\pi m}{h^2} \right)^{3/2} V \int_0^\infty \frac{\sqrt{\epsilon}}{z^{-1} e^{\epsilon/kT} - 1} d\epsilon + \frac{1}{e^{(\epsilon_0 - \mu)/kT} - 1}.
\end{aligned}
$$

For now, however, it will be simpler to just work with N_e which is given by $N_e = N - N_0$. Taking advantage of the change of variable $x = \epsilon/kT$ we can write

$$(1.41) \qquad N_e = \frac{2}{\sqrt{\pi}} \left(\frac{2\pi mkT}{h^2} \right)^{3/2} V \int_0^\infty \frac{\sqrt{x}}{z^{-1} e^x - 1} dx.$$

The next step is to impose the restriction that the occupancy of a given state must be greater than or equal to zero, $n \geq 0$ as it would not be physical to have a negative number of particles in a state. If $z < 0$ the integrand will be negative over the entire range of integration resulting in $N_e < 0$ which clearly cannot describe a physical case. When $z > 1$ as x gets small there will be a value of $x = x_0$ such that $z^{-1} e^x = 1$ which will cause the integrand to blow up, and then for $x < x_0$ the integrand will be negative. Therefore, we may restrict ourselves to $0 \leq z \leq 1$ as fugacities outside of this range to not represent physical situations [17]. Over this range the integral increases monotonically with z and is therefore bounded at $z = 1$. This allows us to write that:

$$(1.42) \qquad N_e \leq \frac{2}{\sqrt{\pi}} \left(\frac{2\pi mkT}{h^2} \right)^{3/2} V \int_0^\infty \frac{\sqrt{x}}{e^x - 1} dx.$$

This integral does not have a nice analytic solution, but including the factor of $2/\sqrt{\pi}$, it is approximately 2.612. We will discuss the value of this integral, the choice to include the factor of $2/\sqrt{\pi}$, and approximations of other integrals of this form later on. For now we will just use this value in our bound for N_e.

The case where

$$(1.43) \qquad N_e = 2.612 \left(\frac{2\pi mkT}{h^2} \right)^{3/2} V.$$

can be interpreted to mean that the excited states have reached their maximum capacity and cannot hold any additional particles. Therefore, at fixed T, and V if more particles are added to the system they will all be forced into the ground state. Alternatively, at fixed N a decrease in T or V will force some particles into the ground state. To consolidate of how these parameters affect N_0 we can define a particle density $\rho \equiv N/V$. Now, a decrease in temperature or an increase in density corresponds to an increase in N_0. This phenomenon of particles being forced into the ground state is known as Bose-Einstein condensation and the condition for it to occur is:

$$(1.44) \qquad N > 2.612 \left(\frac{2\pi mkT}{h^2} \right)^{3/2} V,$$

or that

$$(1.45) \qquad T > T_c \equiv \frac{h^2}{2\pi mkT} \left(\frac{N}{2.612V} \right)^{2/3},$$

Where T_c is the critical or condensation temperature below which Bose-Einstein condensation will occur. Using T_c we can write equation 1.43 in the more useful form:

$$(1.46) \qquad N_e = N \left(\frac{T}{T_c} \right)^{3/2} \qquad (T < T_c).$$

Since $N_0 = N - N_e$ we can write that:

$$(1.47) \qquad N_0 = N \left[1 - \left(\frac{T}{T_c} \right)^{3/2} \right] \qquad (T < T_c).$$

At this point our system has two phases: the thermal phase consisting of N_e, and the the condensed phase consisting of N_0. Figure 1.2 shows how the occupancies of the thermal and condensed phases change as temperature is decreased from $T > T_c$ to $T = 0$. The particles in the condensed phase are referred to as a Bose-Einstein Condensate(BEC).

Established how and under what conditions a BEC will form only prompts more questions. Such as, what are the properties of such a system? Is there anything happening in a BEC that would warrant greater study or the potential to be used for some other purpose? Notice that, excluding the factor of 2.612, T_c is precisely the temperature at which the quantum volume equals the volume per particle, meaning that the particles' wave functions are beginning to overlap, Figure 1.3 is an attempt to depict this. As the process continues the wave functions will gradually become spatially localized. This has the interesting consequence of the particles becoming indistinct. What I mean by this is that not only are the particles indistinguishable, meaning that you cannot tell particle A from particle B, but that you cannot even tell that there are in fact two particles! A BEC can be thought of as a macroscopically large body of completely indistinct matter, because in the limit where $T \to 0$ and $\rho \to \infty$ all of the particles will exist in the same spatial region while exhibiting the same quantum mechanical behavior.
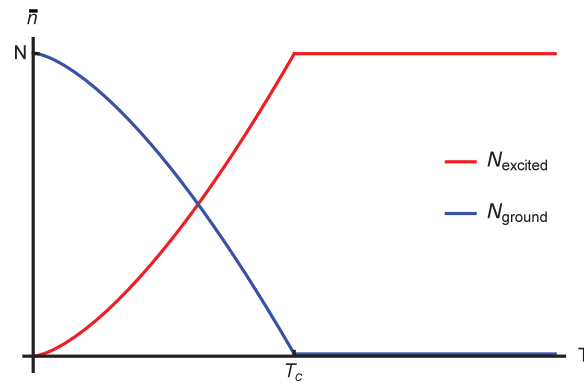
FIGURE 1.2. While $T > T_c$ $N_0 = 0$ and $N_e = N$. As T falls below T_c particles begin to move rapidly to the ground state, thereby condensing.

This behavior is the origin for the description of a BEC being like one "super" atom. A BEC is an inherently quantum mechanical system which is precisely why they are of interest for further study.
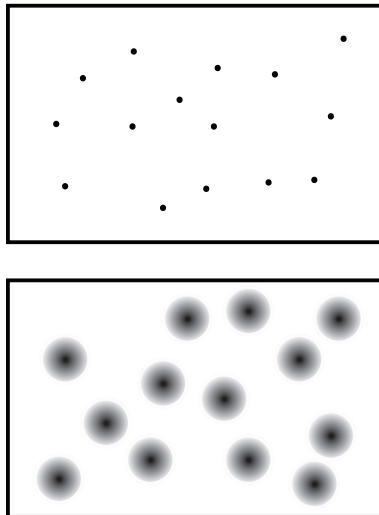

FIGURE 1.3. As the atoms are cooled their de Broglie wavelengths become expand and begin to overlap so that eventually individual atoms become indistinct.

It is interesting to note that on its surface Bose-Einstein condensation seems very similar to a gas condensing into a liquid because the gas cools the number of particles in the ground sate increases disproportionately. It is, however, fundamentally a different process. Vapor condensing is driven inter-particle interactions, specifically an attractive force. Our derivation for Bose-Einstein condensation assumes that the particles are non-interacting. Thus Bose-Einstein condensation is a purely quantum mechanical process as it does not depend on inter-particle interactions.

We have described the processes of Bose-Einstein condensation, and at least hinted at why the resulting BECs are of interest. We will shift our focus to realizing a BEC in lab. This will require reworking some of the theory in order to more appropriately describe the conditions in which we will be able create a BEC in lab.

3.1. BEC in a Harmonic Trap. Our work so far in describing a Bose-Einstein condensation, since introducing $a(\epsilon)$, the density of states, has been in terms of some volume V. Essentially, we have been considering a system of bosons trapped in a box. In lab we do not have an analog to this magic box that we could load with bosons. What we can do instead is to form confining magnetic potentials, or traps. This called magnetic trapping which is discussed in detail in Ch. 4, but for now it is sufficient to know that magnetic traps, to a very good approximation, can be modeled as harmonic potentials. Quantum mechanically the difference between our previous BEC derivation and the situation in lab can be thought of as finding allowed sates of a three dimensional square well potential with a characteristic volume versus the three dimensional harmonic potential that has a characteristic frequency. All we will need to do to appropriately modify our derivation is to consider the density of states for a three dimensional harmonic oscillator instead of a box.

We will consider an isotropic harmonic oscillator with a resonance frequency of ω_0, also known as the trap frequency. The density of states for this potential is

$$(1.48) \qquad b(\epsilon) = \frac{\epsilon^2}{2(\hbar\omega_0)^3}.$$

Moving forward as before we can write N_e as:

$$
\begin{aligned}
N_e &= \int_0^\infty b(\epsilon) \frac{1}{z^{-1}e^{\epsilon/kT} - 1} d\epsilon \\
(1.49) \qquad &= \frac{1}{2(\hbar\omega)^3} \int_0^\infty \frac{\epsilon^2}{z^{-1}e^{\epsilon/kT} - 1} d\epsilon.
\end{aligned}
$$

We can now make the same change of variables, $x = \epsilon/kT$, and find a bound for N_e by the same argument as we used previously which yields:

$$(1.50) \qquad N_e \le \left(\frac{kT}{\hbar\omega_0}\right)^3 \frac{1}{2} \int_0^\infty \frac{x^2}{e^x - 1} dx.$$

The integral once again does not have an analytic solution, but including the factor of $1/2$, it is approximately 1.202. This numeric approximation, and the choice to include the factor of $1/2$ will be discussed directly following this derivation.

Now the excited states will be filled in the case that

$$(1.51) \qquad N_e = 1.202 \left(\frac{kT}{\hbar\omega_0}\right)^3.$$

and our condition for the onset of condensation becomes

$$(1.52) \qquad N \ge 1.202 \left(\frac{kT}{\hbar\omega_0}\right)^3,$$

or

$$(1.53) \qquad T > T_c \equiv \frac{\hbar\omega_0^3}{k} \left(\frac{N_e}{1.202}\right)^{1/3}$$

Finally, we can do the same algebra as before to find that

$$(1.54) \qquad N_0 = N \left[1 - \left(\frac{T}{T_c} \right)^3 \right] \qquad (T < T_c).$$

This is result is clearly analogous to equation 1.47. In fact, they are same excluding a redefined critical temperature in terms of ω_0, and the exponential dependence on the T/T_c ratio increasing to the much stronger power of 3 as opposed to the $3/2$ for bosons in a box.

4. Bose-Einstein Integrals

In the previous two sections we described Bose-Einstein condensation for two different confining potentials, and interestingly the the results turned out to be surprisingly similar. To explain the reason for such strong parallels between the two derivations in this section we are going to take a closer look at the underlying mathematics used in sections 1.3.1 and 1.3.2.

To begin I have rewritten the integrals in equations 1.41 and 1.50 and placed them side by side for comparison.

$$\int_0^\infty \frac{x^{1/2}}{z^{-1}e^x - 1} dx \qquad\qquad \int_0^\infty \frac{x^2}{z^{-1}e^x - 1} dx$$

The similarities between the two integrals are immediately apparent, the only difference being the power of x. They are both integrals of the general form

$$(1.55) \qquad G_s(z) = \int_0^\infty \frac{x^{s-1}}{z^{-1}e^x - 1},$$

which are known as the Bose-Einstein integrals and appear frequently in the study of Bose-Einstein statistics [12]. One reason for this is that the integrand is just the product of the Bose-Einstein distribution and x to some power. In the cases we have considered the power of x is equivalent to that of the energy term in a density of states. Therefore, integrals of form $G_s(z)$ will appear in any expression counting the number of bosons in a system.

4.1. Computing $G_s(1)$. Our previous work depended on numeric approximations of the integrals $\frac{2}{\sqrt{\pi}}G_{3/2}(1)$ and $\frac{1}{2}G_3(1)$. In this section we provide an explanation of how these numeric approximations are obtained. This will require introducing three special functions: the Riemann zeta function $\zeta(s)$, the Gamma function $\Gamma(s)$, and the the polylogarithm $\mathrm{Li}_s(z)$. These functions are defined respectively as [18, 19]:

$$(1.56) \qquad \zeta(s) = \sum_{n=1}^\infty \frac{1}{n^s}, \qquad \mathrm{Re}[s] > 0,$$

and

$$(1.57) \qquad \Gamma(s) = \int_0^\infty x^{s-1}e^{-x}dx, \qquad \mathrm{Re}[s] \neq -1, -2, -3\ldots,$$

and

(1.58)
$$\text{Li}_s(z) = \sum_{n=1}^{\infty} \frac{z^n}{n^s}, \qquad s \in \mathbb{C}.$$

Additionally, $\text{Li}_s(z)$ has the following integral representation:

(1.59)
$$\text{Li}_s(z) = \frac{z}{\Gamma(s)} \int_0^{\infty} \frac{x^{s-1}}{e^x - z} dx, \qquad \text{Re}[s] > 0.$$

Now that we have the required tools to move forward, let's consider

(1.60)
$$\lim_{z \to 0} G_n(s) = \int_0^{\infty} z e^{-x} x^{s-1} dx = z\Gamma(s).$$

This suggests that it might be useful to define a new function $g_n(z)$, sometimes called the Bose-Einstein function, such that

(1.61)
$$G_n(z) = g_n(z)\Gamma(n).$$

Now writing $g_n(z)$ in terms of $G_n(z)$ results in

$$
\begin{aligned}
g_n(z) &= \frac{1}{\Gamma(n)} \int_0^{\infty} \frac{x^{s-1}}{z^{-1}e^x - 1} dx \\
&= \frac{1}{\Gamma(n)} \int_0^{\infty} \frac{x^{s-1} z e^{-x}}{1 + z e^{-x}} dx \\
&= \frac{1}{\Gamma(n)} \int_0^{\infty} x^{s-1} \sum_{n=1}^{\infty} (z e^{-x})^n dx.
\end{aligned}
$$
(1.62)

The step from the second line to the third line requires recognizing the form of a geometric series multiplied by its common ratio. The starting point of the index on the summation is adjusted to account for this extra factor of the ratio. The sum in the integrand has the closed form

(1.63)
$$\sum_{n=1}^{\infty} (z e^{-x}) = \frac{z}{e^x - z}.$$

Replacing the sum we can write that

$$
\begin{aligned}
g_n(z) &= \frac{z}{\Gamma(n)} \int_0^{\infty} \frac{x^{s-1}}{e^x - z} dx \\
&= \text{Li}_s(z) \\
&= \sum_{n=1}^{\infty} \frac{z^n}{n^s} \\
&= z + \frac{z^2}{2^s} + \frac{z^3}{3^s} \dots.
\end{aligned}
$$
(1.64)

Considering the first few terms of $g_n(z)$ it is clear that as $z \to 0$, $g_n(z) \to z$. This means that our definition of $g_n(z)$ will reproduce equation 1.61, exactly as we should hope. In the case where $z = 1$

$$
\begin{aligned}
g_n(1) &= \sum_{n=1}^{\infty} \frac{1}{n^s} \\
&= \zeta(s)
\end{aligned}
$$

(1.65)

The method used to approximate the integrals in equations 1.41 and 1.50 was to write them in the form of $g_n(z)$ using that $\Gamma(3/2) = \sqrt{\pi}/2$ and $\Gamma(3) = 2$. Then by equation 1.64 the integrals reduce to $\zeta(s)$ when $z = 1$. The Riemann zeta for $s = 3/2$ and $s = 3$ has approximate values of $\zeta(3/2) \approx 2.612$ and $\zeta(3) \approx 1.202$. The goal earlier was not to allow that mathematics distract from the physics, but now the results in the previous section could be written more precisely in terms of $\zeta(s)$ as

(1.66)
$$
T > T_c \equiv \frac{\hbar \omega_0^3}{k} \left(\frac{N_e}{\zeta(3/2)} \right)^{2/3},
$$

and

(1.67)
$$
T > T_c \equiv \frac{\hbar \omega_0^3}{k} \left(\frac{N_e}{\zeta(3)} \right)^{1/3},
$$

for the box and harmonic oscillator respectively.

4.2. Generalizing for any Density of States. Now that we have a solution to $g_n(z)$ we can generalize our work done earlier for any density of states. In general a density of states $c(\epsilon)$ has the form

(1.68)
$$
c(\epsilon) = C \epsilon^{s-1},
$$

where C is some real constant determined by the confining potential and ϵ is energy whose power is also depends the potential. As we said earlier

$$
\begin{aligned}
N_e &= \int_0^{\infty} \frac{c(\epsilon)}{z^{-1} e^{\epsilon/kt} - 1} d\epsilon \\
&= C \int_0^{\infty} \frac{\epsilon^{s-1}}{z^{-1} e^{\epsilon/kt} - 1} d\epsilon \\
&= C(kT)^s \int_0^{\infty} \frac{x^{s-1}}{z^{-1} e^{\epsilon/kt} - 1} dx.
\end{aligned}
$$

(1.69)

The last line is obtained by making the change of variables, $x = \epsilon/kT$, as before. Now we will apply the condition that $z = 1$, to consider the case where the excited states are full and condensation must occur and find that

$$
\begin{aligned}
N_e &= C(kT)^s \int_0^\infty \frac{x^{s-1}}{e^{\epsilon/kt} - 1} dx \\
&= C(kT)^s \Gamma(s) \frac{1}{\Gamma(s)} \int_0^\infty \frac{x^{s-1}}{e^{\epsilon/kt} - 1} dx \\
&= C(kT)^s \Gamma(s) g_n(1) \\
&= C(kT)^s \Gamma(s) \zeta(s).
\end{aligned}
$$

(1.70)

This means that in general the condition for Bose-Einstein condensation to occur is

(1.71)
$$
N > C(kT)^s \Gamma(s) \zeta(s),
$$

or

(1.72)
$$
T > T_c \equiv \frac{1}{k} \left(\frac{N}{C\Gamma(s)\zeta(s)} \right)^{1/s}.
$$

From here we can write N_e in terms of T_c which results in

(1.73)
$$
N_e = N \left(\frac{T}{T_c} \right)^s.
$$

Finally, from here we can generalize our expression for N_0 the number of atoms in a condensate.

(1.74)
$$
N_0 = N \left[1 - \left(\frac{T}{T_c} \right)^s \right]
$$

Interestingly the dependence on the T/T_c goes as one plus the exponent of the energy term in $c(\epsilon)$. For a more rigorous description of this generalization as well as considerations of other confining potentials see [20]. We have now described the process of Bose-Einstein condensation for two specific cases and in general along with a brief overview of some of the underlying mathematics. In the next section we will develop a simple model for describing a BEC itself.

5. The Thomas-Fermi Approximation

So far we established that a system of bosons will condense to the ground state if certain conditions are met. We have not yet discussed any properties of the condensate itself. Our previous work has assumed non-interacting bosons, in this section we will make use of the inter-particle interactions, that must be present in a real condensate, in order to describe the size of the shape of a condensate. As we will see this method also provides a means by which to distinguish the condensed phase from the thermal phase. To do this we will follow the work presented in [21, 14].

A result from scattering theory is that the energy due to inter-particle interactions can be accounted for by adding a term proportional to $|\psi|^2$ to the Hamiltonian for the system [14].

(1.75)
$$
H = \frac{\hbar^2}{2M} \nabla^2 + V(\boldsymbol{r}) + g|\psi|^2,
$$

where

$$(1.76) \qquad g = \frac{4\pi\hbar^2 N_0 a}{M}.$$

The resulting time-independent Schrödinger equation is

$$(1.77) \qquad \left[\frac{\hbar^2}{2M}\nabla^2 + V(\boldsymbol{r}) + g|\psi|^2\right]\psi = \mu\psi.$$

This is called the Gross-Pitaevskii equation. As Foot suggests one could continue from here by applying the variational method to obtain an approximation for the ground state energy and calculate the size of the condensate from there, but there is an easier approach. In order to achieve condensation temperature must decrease and density must increase. As temperature decreases kinetic energy decreases and as density increases $|\psi|^2$ increases. So in a condensate the kinetic contribution to the total energy gets small while the interaction contribution gets large [14]. On this basis we will take the kinetic term in H to be negligible, and equation 1.77 becomes

$$(1.78) \qquad \left[V(\boldsymbol{r}) + g|\psi|^2\right]\psi = \mu\psi.$$

Therefore, in the region where $\psi \neq 0$, which is where the condensate is located

$$(1.79) \qquad |\psi|^2 = \frac{\mu - V(r)}{g}.$$

Treating the kinetic energy as negligible is called the Thomas-Fermi approximation and it is valid in the so called Thomas-Fermi regime. Experimentally we do not measure $|\psi(r)|^2$ the probability of finding a particle at a given point directly, but rather number density $n(r)$ of the system which can be written as

$$(1.80) \qquad \begin{aligned} n(r) &= N_0|\psi(r)|^2 \\ &= n_0\left(1 - \frac{V(r)}{\mu}\right), \end{aligned}$$

where $n_0 = N_0\mu/g$, the density at the center of the condensate. As mentioned previously, our BECs will formed in traps that can be described as harmonic oscillator so we will consider the potential of a three dimensional harmonic oscillator

$$(1.81) \qquad V(r) = \frac{1}{2}M(\omega_x^2 x^2 + \omega_y^2 y^2 + \omega_z^2 z^2).$$

Applying this potential to equation 1.80 we find that:

$$(1.82) \qquad n(r) = n_0\left(1 - \frac{x^2}{R_x^2} - \frac{y^2}{R_y^2} - \frac{z^2}{R_z^2}\right),$$

where

(1.83)
$$R_i = \sqrt{\frac{2\mu}{M\omega_i^2}} \Rightarrow \mu = \frac{1}{2}M\omega_i^2 R_1^2 \qquad i = x, y, z.$$

From equation 1.82 we can see that the condensate will have the shape of an inverted parabola in all three directions and will therefore be ellipsoidal. Equation 1.83 shows that the atoms fill up a trap to μ which is the chemical potential of the system as it is the energy associated with adding or removing one particle from the system.

The kinetic energy of thermal atoms in general cannot be ignored and because they are less dense their inter-particle interactions are less significant. To a good a approximation $|\psi|^2$ for thermal atoms can be described by a Gaussian, which are the allowed sates of non-interacting particles in a harmonic oscillator. So the density distribution of a cloud thermal atoms will be fit well by a simple Gaussian. On the other had because condensed atoms enter the Thomas-Fermi regime a cloud that has atoms in both the thermal and condensed phases can be described by a function that has the form of an inverted parabola around the origin and is Gaussian on the sides. This is precisely the method used in many BEC experiments to determine if a condensate is in fact present and if so how large it is.

Atom-Light Interactions

We have now explored Bose-Einstein condensation, providing an answer to our first question: what is a BEC? Our second question is: what techniques can we use to make a BEC? However, the first part of the answer to this question, in Ch. 3, relies heavily on atom-light interactions. So before beginning to answer this question it is necessary to take a detour and investigate closely these interactions between atoms and electromagnetic radiation. I have decided that it will be less disruptive to our general line of inquiring to place this material here so that when in Ch. 3 we need to make use of the results in this chapter we can due so, as opposed to being to forced to halt our progress and derive them at the time.

Our ultimate goal in this chapter is to find an expression for the scattering rate, R_{scatt}, of a system of atoms. This is rate at which atoms emit or scatter photons when exposed to a near-resonant monochromatic radiation field. A monochromatic radiation field is just a more complicated way to say "light from a laser". There are two common methods for the deriving an expression for R_{scatt}. The first is a purely classical description known as the Lorentz model in which an atom and an electron are modeled as a driven damped harmonic oscillator where the radiation provides that driving force. The second is a semi-classical approach in which the atom is treated quantum mechanically and the radiation in treated as a classical field. The two methods yield equivalent results for near resonant interaction, precisely the regime we are concerned with. However, the semi-classical approach is more theoretically rigorous, and less manipulation of the result is required to write R_{scatt} in its most useful form. Furthermore, although it is a purely classical analysis of the situation the Lorentz model does not require significantly less work than the semi-classical analysis. For all of these reasons, we will proceed with the semi-classical description. This derivation has been developed from the work presented in [**14, 22, 23**]. If the reader desires [**24**] provides a thorough derivation of the Lorentz model.

1. Two-Level System

We will start from the time-dependent Schrödinger equation

$$(2.1) \qquad i\hbar\frac{\partial\Psi}{\partial t} = H\Psi.$$

where Ψ is the time-dependent wave function, and H is the Hamiltonian of the system. We will express the Hamiltonian as $H = H^0 + H'(t)$ where H^0 is the unperturbed Hamiltonian and $H'(t)$ is some time-dependent perturbation.

Before introducing the electromagnetic radiation as a time-dependent perturbation we are going to limit ourselves to two-level system as shown in Figure 2.1. This system is composed of an atom that has two allowable states: a ground state $|g\rangle$ and one excited state $|e\rangle$. Although this may seem arbitrarily restrictive the behavior of many atoms behave as two-level systems to a good approximation. Yet, it is not perfect and one particular instance where the theory

developed in this chapter breaks down will be mentioned in Ch. 3 as part of the discussion of optical molasses and the Doppler limit.
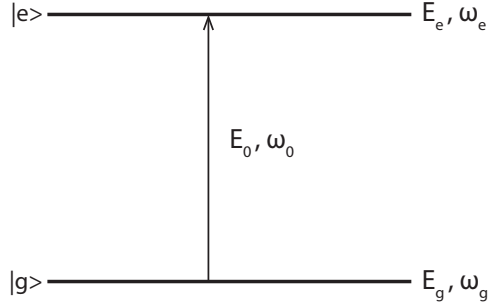

FIGURE 2.1. A two-level system is comprise of the two states $|g\rangle$ and $|e\rangle$. Each state has an associated energy and frequency.

From introductory quantum mechanics we write the time evolution of each of the two states as

$$
\begin{aligned}
\Psi_g(\boldsymbol{r}, t) &= |g\rangle\, e^{-iE_g t/\hbar} \\
\Psi_e(\boldsymbol{r}, t) &= |e\rangle\, e^{-iE_e t/\hbar},
\end{aligned}
$$
(2.2)

where E_g and E_e are given by

$$
\begin{aligned}
H^0 |g\rangle &= E_g |g\rangle \\
H^0 |e\rangle &= E_e |e\rangle .
\end{aligned}
$$
(2.3)

Since there are only two states we need only to consider the two-dimensional Hilbert space which $|g\rangle$ and $|e\rangle$ form a basis set. So we can write the generalized wave function as

$$
\Psi(\boldsymbol{r}, t) = c_g |g\rangle\, e^{-i\omega_g t} + c_e |e\rangle\, e^{-i\omega_e t},
$$
(2.4)

where I have introduced that $\omega_n = E_n/\hbar$, $n = g, e$. Normalization requires that the coefficients c_g and c_e satisfy

$$
|c_g|^2 + |c_e|^2 = 1.
$$
(2.5)

Now we have a good description of the electron's unperturbed state which exists when there is no incident radiation on the atom. Now turning on our laser, electric field $\boldsymbol{E} = \boldsymbol{E}_0 \cos(\omega t)$ of the radiation incident on the atom will introduce a perturbation described by

$$
H'(t) = e\boldsymbol{r} \cdot \boldsymbol{E}_0 \cos(\omega t)
$$
(2.6)

Now we plug equation 2.4 into the time-dependent Schrödinger equation which yields:

$$
(2.7) \quad i\hbar \left[\dot{c}_g |g\rangle\, e^{-i\omega_g t} + \dot{c}_e |e\rangle\, e^{-i\omega_e t} + c_g |g\rangle \left(-\frac{iE_g}{\hbar} \right) e^{-i\omega_g t} + c_e |e\rangle \left(-\frac{iE_e}{\hbar} \right) e^{-i\omega_e t} \right]
$$
$$
= c_g [H^0 |g\rangle] e^{-i\omega_g t} + c_e [H^0 |e\rangle] e^{-i\omega_e t} + c_g [H' |g\rangle] e^{-i\omega_g t} + c_e [H' |e\rangle] e^{-i\omega_e t}.
$$

Fortunately we can use equations 2.3 to realize that the last two terms on the left side are equal to the first two terms on the right side. After canceling those four terms we are left with the slightly simpler equation

$$(2.8) \qquad i\hbar \left[\dot{c}_g \left| g \right\rangle e^{-i\omega_g t} + \dot{c}_e \left| e \right\rangle e^{-i\omega_e t} \right] = c_g [H' \left| g \right\rangle] e^{-i\omega_g t} + c_e [H' \left| e \right\rangle] e^{-i\omega_e t}.$$

To isolate $\dot{c}_g$ and $\dot{c}_e$ we can take the inner product with respect to $\left| g \right\rangle$ and $\left| e \right\rangle$ respectively. This is done simply by multiplying through by either $\left\langle g \right|$ or $\left\langle e \right|$. This process results in the following pair of first-order coupled ordinary differential equations:

$$
\begin{aligned}
i\dot{c}_g &= \frac{1}{\hbar} H'_{ge} e^{-i\omega_0 t} c_e, \\
(2.9) \qquad i\dot{c}_e &= \frac{1}{\hbar} H'_{ge} e^{i\omega_0 t} c_g,
\end{aligned}
$$

where $\omega_0 = \omega_e - \omega_g$ which is the frequency associated with the energy difference between $\left| e \right\rangle$ and $\left| g \right\rangle$ and $H'_{ij} = \left\langle i \right| H' \left| j \right\rangle$. Finally substituting equation 2.6 for H' results in:

$$
\begin{aligned}
i\dot{c}_g &= \Omega \cos(\omega t) e^{-i\omega_0 t} c_e, \\
(2.10) \qquad i\dot{c}_e &= \Omega^* \cos(\omega t) e^{i\omega_0 t} c_g,
\end{aligned}
$$

where the Rabi frequency Ω is defined as

$$(2.11) \qquad \Omega \equiv \frac{\left\langle g \right| e\boldsymbol{r} \cdot \boldsymbol{E}_0 \left| e \right\rangle}{\hbar} = \frac{-eE_0}{\hbar} \left\langle e \right| r \left| g \right\rangle = \frac{-\mu E_0}{\hbar},$$

where μ is the induced dipole moment. In order to keep progressing with an analytic solution when we need to make use of these equations in future sections we must introduce the rotating wave approximation to equations 2.10. This is nothing more than applying the original stipulation that we are considering near-resonant radiation. The first step is to rewrite the $\cos(\omega t)$ terms using Euler's formula

$$
\begin{aligned}
i\dot{c}_g &= \frac{\Omega}{2} \left(e^{i(\omega - \omega_0)t} + e^{-i(\omega + \omega_0)t} \right) c_e, \\
(2.12) \qquad i\dot{c}_e &= \frac{\Omega^*}{2} \left(e^{i(\omega + \omega_0)t} + e^{-i(\omega - \omega_0)t} \right) c_g.
\end{aligned}
$$

Since we are limiting ourselves to near-resonant radiation $\omega + \omega_0 \sim 2\omega_0$. Therefore, the $(\omega + \omega_0)t$ term oscillates very fast as compared to $(\omega - \omega_0)t$. On this basis we will approximate that the $(\omega + \omega_0)t$ average to zero. This allows us write equations 2.12 as:

$$
\begin{aligned}
i\dot{c}_g &= \frac{\Omega}{2} e^{i\delta t} c_e, \\
(2.13) \qquad i\dot{c}_e &= \frac{\Omega^*}{2} e^{-i\delta t} c_g,
\end{aligned}
$$

where the detuning $\delta = \omega - \omega_0$.

We have now described the time evolution of our two-level system, but for one problem. Since an excited state is not a stationary state an excited atom will eventually fall back down or decay to the ground state by spontaneously emitting a photon. This process is called spontaneous

emission and leads to a flaw in our work so far. According to our current equations if the laser is turned off $E_0 = 0 \Rightarrow \dot{c}_g = \dot{c}_e = 0$. This means that when the laser is turned off all atoms in $|e\rangle$ will stay there despite the fact that we know they must decay from $|g\rangle$ to $|e\rangle$. Some authors use this simple argument to justify adding decay terms into equations 2.10, or into comparable equations later on in the derivation, that depend on c_g and c_e to correct for this. However, with a more careful consideration of spontaneous emission we can develop analytic expressions for these decay terms and explicitly demonstrate how they relate to c_g and c_e.

2. Spontaneous Emission

The idea of spontaneous emission was first proposed by Einstein when he studied Plank's blackbody spectrum. We now know that the cause of spontaneous emission is due to a coupling between the atom and the electromagnetic vacuum field. At the time Einstein developed what are known as the Einstein A and B coefficients which represent the rate of transitions from one state to another and the constant of proportionality between this rate and energy density to describe spontaneous emission. Although he is ultimately correct the method does not provide a description of the process by which spontaneous emission occurs. This was instead accomplished by Victor Weisskopf and his advisor Eugene Wigner in what is now called the Weisskopf-Wigner theory. This section follows their work with the goal of describing the decay from $|e\rangle$ to $|g\rangle$ as presented in [**22, 25**].

Just as before we will consider a two-level atom. This time, however, we will also keep track of the state of the vacuum field's state, by tracking the photons present in the field. So our entire system includes both the atom and the vacuum. We will start with the system in state $|e, 0\rangle$, meaning that the atom is in the excited state and there are no photons present in the field. After the atom decays the state of the system is $|g, 1_S\rangle$, meaning that the atom is in the ground state and there is one photon present in the field emitted in mode $S = (\boldsymbol{k}, \boldsymbol{\epsilon})$, where $\boldsymbol{k}$ is the wave vector indicting the direction the photon was emitted and $\boldsymbol{\epsilon}$ is the polarization vector of the photon. Now, analogously to equation 2.4, we can write that

$$(2.14) \qquad \Psi(t) = c_{e0}(t)e^{-i\omega_0 t}|e, 0\rangle + \sum_S c_{g1_S}(t)e^{-i\omega_k t}|g, 1_S\rangle,$$

where ω_0 is the same as previously $\omega_k = ck$, the frequency of an emitted photon. Now, using the same method as in the previous section we can substitute equation 2.14 into the time-dependent Schrödinger equation, and remove the terms duplicated on both sides of the equation. Then expressions for $\dot{c}_{g1_S}$ and $\dot{c}_{e0}$ can be found by taking the inner product with respect to $|g, 1_S\rangle$ and $|e, 0\rangle$ and respectively. These products results in:

$$(2.15) \qquad i\dot{c}_{g1_S}(t) = c_{e0}(t)\Omega_S^* e^{i(\omega_k - \omega_0)t},$$

and

$$(2.16) \qquad i\dot{c}_{e0}(t) = \sum_S c_{g1_S}(t)\Omega_S e^{-i(\omega_k - \omega_0)t}.$$

where Ω_S is the vacuum Rabi frequency and defined as:

$$(2.17) \qquad \Omega_S \equiv \frac{-\boldsymbol{\mu} \cdot \boldsymbol{E}_{\omega_k}}{\hbar}.$$

In this expression the dipole moment $\boldsymbol{\mu} = e \langle e | \boldsymbol{r} | g \rangle$ and the electric field per mode derives from the classical expression for energy density as:

$$(2.18) \qquad \boldsymbol{E}_{\omega_k} = \sqrt{\frac{\hbar \omega_k}{2\epsilon_0 V}} \hat{\boldsymbol{\epsilon}}$$

where V is the volume used to quantize the field [**26**].

To solve equations 2.15 and 2.16 we will first directly integrate equation 2.15 as

$$(2.19) \qquad c_{g1_S}(t) = i\Omega_S^* \int_0^t c_{e0}(t') e^{i(\omega_k - \omega_0)t'} dt'.$$

Plugging this result into equation 2.16 we find that:

$$(2.20) \qquad \dot{c}_{e0}(t) = -\sum_S |\Omega_s|^2 \int_0^t c_{e0}(t') e^{-i(\omega_k - \omega_0)(t-t')} dt'.$$

Our strategy moving forward will be to convert the sum to an integral, then consider the two integrals separately, and finally take the product of the two results to find a simplified form of $\dot{c}_{e0}(t)$.

To convert the sum to an integral we will consider it in the continuum limit, $V \to \infty$. In this case we can write that:

$$(2.21) \qquad \sum_S = \sum_{\boldsymbol{k}, \boldsymbol{\epsilon}} = \sum_{\epsilon=1}^2 \int \mathcal{D}(k) d^3 k,$$

where $\mathcal{D}(k)$ is the density of states in k-space and limits of the sum over ϵ are justified because the photon is polarized with respect to two axes, $\boldsymbol{\epsilon} = \epsilon_1 \hat{\boldsymbol{k}}_1 + \epsilon_2 \hat{\boldsymbol{k}}_2$, where $\hat{\boldsymbol{k}}_1$ and $\hat{\boldsymbol{k}}_2$ are unit vectors in the plane orthogonal to $\boldsymbol{k}$. Since $\boldsymbol{k}$ is quantized as $k_i = 2\pi n/L$, with $i = x, y, z$ there is one state in a volume $(2\pi/L)^3 = (2\pi)^3/V$, therefore $\mathcal{D}(k) = V/(2\pi)^3$. Now using the spherical coordinates (k, θ, ϕ) with $d^3 k = k^2 \sin(\theta) dk d\theta d\phi$ we can continue from equation 2.21 and find that:

$$(2.22) \qquad \sum_S = \sum_{\epsilon=1}^2 \int_0^\infty k^2 dk \int_0^\pi \sin(\theta) d\theta \int_0^{2\pi} d\phi$$

Having successfully converted the sum to an integral we will now compute the sum in equation 2.20 as follows:

$$(2.23) \qquad \sum_{\boldsymbol{k}, \boldsymbol{\epsilon}} |\Omega_s|^2 = \sum_{\boldsymbol{k}, \boldsymbol{\epsilon}} \frac{\omega_k}{2\epsilon_0 V \hbar} (\boldsymbol{\mu} \cdot \boldsymbol{\epsilon})^2 = \int_0^\infty k^2 \frac{\omega_k}{2(2\pi)^3 \epsilon_0 \hbar} \left[\sum_{\epsilon=1}^2 \int_0^\pi \sin\theta d\theta \int_0^{2\pi} (\boldsymbol{\mu} \cdot \boldsymbol{\epsilon})^2 d\phi \right].$$

Working with just the term in brackets and breaking $\boldsymbol{\epsilon}$ into into its components results in:

$$(2.24) \qquad \sum_{\epsilon=1}^2 \int_0^\pi \sin\theta d\theta \int_0^{2\pi} (\boldsymbol{\mu} \cdot \boldsymbol{\epsilon})^2 d\phi = \int_0^\pi \sin\theta d\theta \int_0^{2\pi} \left[(\boldsymbol{\mu} \cdot \boldsymbol{\epsilon}_{\boldsymbol{k_1}})^2 + (\boldsymbol{\mu} \cdot \boldsymbol{\epsilon}_{\boldsymbol{k_2}})^2 \right] d\phi.$$

To further simplify the dot products we will take a brief stroll into some vector calculus using $\hat{\boldsymbol{k}}_1, \hat{\boldsymbol{k}}_2$, and $\hat{\boldsymbol{k}}_3$, where $\boldsymbol{k} = k\hat{\boldsymbol{k}}_3$ and the other two unit vectors span the plane orthogonal to $\boldsymbol{k}$, as described earlier. Thinking classically this using the direction of propagation along with the two axes of polarization as an orthonormal basis set. More to the point using this basis set we can write that:

$$
\begin{aligned}
\boldsymbol{\mu} &= (\boldsymbol{\mu} \cdot \hat{\boldsymbol{k}}_1)\hat{\boldsymbol{k}}_1 + (\boldsymbol{\mu} \cdot \hat{\boldsymbol{k}}_2)\hat{\boldsymbol{k}}_2 + (\boldsymbol{\mu} \cdot \hat{\boldsymbol{k}}_3)\hat{\boldsymbol{k}}_3 \\
|\boldsymbol{\mu}|^2 &= (\boldsymbol{\mu} \cdot \hat{\boldsymbol{k}}_1)^2 + (\boldsymbol{\mu} \cdot \hat{\boldsymbol{k}}_2)^2 + (\boldsymbol{\mu} \cdot \hat{\boldsymbol{k}}_3)^2 \\
|\boldsymbol{\mu}|^2 - (\boldsymbol{\mu} \cdot \hat{\boldsymbol{k}}_3)^2 &= (\boldsymbol{\mu} \cdot \hat{\boldsymbol{k}}_1)^2 + (\boldsymbol{\mu} \cdot \hat{\boldsymbol{k}}_2)^2 \\
|\boldsymbol{\mu}|^2 \sin^2 \theta &= (\boldsymbol{\mu} \cdot \hat{\boldsymbol{k}}_1)^2 + (\boldsymbol{\mu} \cdot \hat{\boldsymbol{k}}_2)^2
\end{aligned}
$$

(2.25)
.

The last line is achieved by choosing to orient the spherical axes of our coordinate system to be in the direction of $\boldsymbol{\mu}$, which we can do without loss of generality. Now it is a simple matter to evaluate the integrals in 2.24, which results in:

$$
(2.26) \qquad \sum_{\epsilon=1}^{2} \int_0^\pi \sin\theta d\theta \int_0^{2\pi} (\boldsymbol{\mu} \cdot \boldsymbol{\epsilon})^2 d\phi = \frac{8\pi}{3}|\boldsymbol{\mu}|^2.
$$

Finally, by using the change of variables $\omega_k = ck$, we can write the summation in equation 2.20 as:

$$
(2.27) \qquad \sum_S |\Omega_s|^2 = \frac{|\boldsymbol{\mu}|^2}{6\pi^2 \epsilon_0 \hbar c^3} \int_0^\infty \omega_k^3 d\omega_k.
$$

Now we will shift our focus to the integral in equation 2.20. Evaluating this integral requires some careful approximation. We will assume that $c_{e0}(t')$ varies at a rate $\Gamma \ll \omega_0$. The integral makes non-zero contributions when $t \sim t'$. On this basis we can replace $c_{e0}(t')$ with $c_{e0}(t)$ and pull it out of the integral, which becomes

$$
(2.28) \qquad \int_0^t c_{e0}(t') e^{-i(\omega_k - \omega_0)(t-t')} dt' \approx c_{e0}(t) \int_0^t e^{-i(\omega_k - \omega_0)(t-t')} dt'.
$$

Since $\Gamma \ll \omega_0$, we are only interested in $t \gg \omega_0$. This allows us to let the upper limit of the integral approach ∞. Applying these conditions we find that:

$$
(2.29) \qquad c_{e0}(t) \int_0^\infty e^{-i(\omega_k - \omega_0)(t-t')} dt' = \pi\delta(\omega_k - \omega_0) - i\mathcal{P}\left(\frac{1}{\omega_k - \omega_0}\right),
$$

where $\mathcal{P}$ represents the Cauchy principle part. Since $\mathcal{P}$ is purely imaginary it only contributes a phase shift and we will ignore it here. We can do this because we are primarily concerned with the time derivatives of c_{e0} and c_{g1_S} which must be in phase with each other, so for our purposes a phase shift just represents a change of origin. Putting our results of the sum and integral terms in equation 2.20 together we find that:

$$
(2.30) \qquad \dot{c}_{e0}(t) = -\frac{\Gamma}{2}c_{e0}(t),
$$

where

$$\Gamma = \frac{\omega_0^3 |\boldsymbol{\mu}|^2}{3\pi\epsilon_0 \hbar c^3}. \tag{2.31}$$

We will see in the next section that Γ is the decay rate of the population of atoms in the excited state. Doing so requires furthering our work so that we can consider and ensemble of two-level atoms, instead of just one.

3. Density Matrix

Our work until this point has only dealt with pure states. These are states that can be expressed with a single ket as $|\Psi\rangle$. Since we have only been considering a system consisting of one atom its state can always be described by equation 2.4 which is to say that the system is in either $|g\rangle$, $|e\rangle$, or some linear combination of the two. If our ultimate goal were to study singular atoms this would be sufficient. However, since we hope to progress to laser cooling and later Bose-Einstein condensation we must describe the behavior of an entire ensemble of atoms in a radiation field.

In quantum mechanics there are two kinds of ensembles, pure and mixed. A pure ensemble is one in which every atom is in the same state, which is certainly a special case. In a mixed ensemble atoms are free to exist in any given $|\Psi\rangle$. This is the case we must consider because in general there is no reason why a group of our two-level atoms should all be in the same state. At this point it may seem like we need throw out our previous work and start again, but fortunately each atom on an individual basis can still be said to be in a pure state $|\Psi\rangle$, as defined earlier. In this way a mixed state can be thought of as mixture of pure states. So we should be able to describe our mixed ensemble in terms of each of its members. In this section we present the density operator as a means by which to accomplish this following the presentations in [**14, 22, 27, 28, 29**]

3.1. An Introduction to the Density Matrix. When considering a pure quantum mechanical state it is common practice to describe the system in terms of expectation values:

$$\langle A \rangle = \langle \Psi | A | \Psi \rangle. \tag{2.32}$$

This approach works well when the situation is limited to pure states, but will not work well when attempting to use to many pure state to describe an mixed one. In order accomplish this we need to introduce the density operator

$$\rho \equiv |\Psi\rangle \langle \Psi|. \tag{2.33}$$

We can write any pure state and its conjugate as

$$|\Psi\rangle = \sum_{i=1}^{n} c_i |\psi_i\rangle, \tag{2.34}$$

and

$$\langle \Psi | = \sum_{i=1}^{n} c_i^* \langle \psi_i|, \tag{2.35}$$

where $\{\psi_i\}$ forms a basis set and $\sum_{i=1}^{n} |c_i|^2 = 1$. This allows us to say that the elements of the density matrix are given by

$$(2.36) \qquad \rho_{i,j} = \langle\psi_i| \, \rho \, |\psi_j\rangle = \langle\psi_i|\Psi\rangle \, \langle\Psi|\psi_j\rangle = c_i c_j^*.$$

Thus far we still have just a description of a pure state $|\Psi\rangle$. However, since each atom is described by a pure state we are actually trying to describe an ensemble of states $|\Psi_i\rangle$, each with some fractional probability p_i. So the entire system can be described by a sum of pure state density matrices as

$$(2.37) \qquad \rho = \sum_{i=1}^{n} p_i \, |\Psi_i\rangle \, \langle\Psi_i| \, .$$

Now we are ready to consider an ensemble of two-level atoms for which the density matrix for a pure state can be written as

$$(2.38) \qquad \rho \equiv |\Psi\rangle \, \langle\Psi| = \begin{pmatrix} c_g \\ c_e \end{pmatrix} \begin{pmatrix} c_g^* & c_e^* \end{pmatrix} = \begin{pmatrix} |c_g|^2 & c_g c_e^* \\ c_e c_g^* & |c_e|^2 \end{pmatrix} = \begin{pmatrix} \rho_{gg} & \rho_{ge} \\ \rho_{eg} & \rho_{ee} \end{pmatrix}.$$

Now that we have a specific density matrix it is easier to understand the meanings of the individual terms. The diagonal elements are called the densities and represent the probability of finding a particle in either $|e\rangle$ or $|g\rangle$. The off-diagonal terms are called the coherences and in general represent the response of the system to the frequency a perturbation. In our case we are interested in considering the perturbation due to the radiation field of a laser, so the coherences will depend on ω the frequency of the laser. This concept is more clearly illustrated if we consider the form of the dipole moment $\boldsymbol{p}$ induced in an atom by the radiation field. Choosing to align our coordinate system such that $\boldsymbol{E} = E_o \cos(\omega t)\hat{\boldsymbol{z}}$ we can write that

$$
\begin{aligned}
\langle p\rangle = \langle -ez\rangle &= -e \int \Psi^*(t) z \Psi(t) d^3\boldsymbol{r} \\
&= -e \int \left(c_g \, |g\rangle \, e^{-i\omega_g t} + c_e \, |e\rangle \, e^{-i\omega_e t} \right)^* z \left(c_g \, |g\rangle \, e^{-i\omega_g t} + c_e \, |e\rangle \, e^{-i\omega_e t} \right) d^3\boldsymbol{r} \\
(2.39) \qquad &= -e \left(c_e c_g^* \, \langle\psi_e| \, z \, |\psi_g\rangle \, e^{i\omega_0 t} + c_g c_e^* \, \langle\psi_g| \, z \, |\psi_e\rangle \, e^{-i\omega_0 t} \right).
\end{aligned}
$$

So the coherences determine the magnitude of $\boldsymbol{p}$ which can also be thought of as the strength of the coupling between the atom and the radiation field. The greater the dipole moment the greater the coupling.

In our model atoms scatter a photons due to spontaneous emission induced $|e\rangle \to |g\rangle$ transitions, which cause a change over time in the populations of the two states. By this logic R_{scatt} will depend on how the density matrix evolves in time. So moving forward our task will be to derive expressions for the time derivatives of the elements of ρ. Equation 2.37 describes just one of the many pure states represented in the mixed ensemble and does not describe the entire statistical mixture. However, we are primarily concerned with the time dependence of the density matrix, which in is given as

$$(2.40) \qquad i\hbar \frac{d\rho}{dt} = [H, \rho].$$

Since we are considering an ensemble of identical atoms in the same field the density matrix of each pure sate will evolve over time in the same way, which is to say that $\dot{\rho}$ is the same for all pure states. Thus it is valid to describe the time evolution of the entire system in terms of the time derivative of a singular pure state.

In the previous two sections we have considered the coupling between the two-level atom system, a near-resonant radiation field, and the vacuum field. We can now represent this coupling in terms of two density matrices, each one due to the coupling of one field in the absence of the other. Working with two separate sets of equations due to each field would be a terrible nuisances, so instead we will consider the coupling due to the net field which is just the superposition of the two fields. In practice this means that we can simply add the elements each density matrix to find the density matrix due to the presence of both fields. In general this combination of density matrices can be written as

$$(2.41) \qquad \rho_{net} = \rho_{rad} + \rho_{vac} = \sum_{i=1}^{n} p_i \rho_{rad_i} + \sum_{i=1}^{n} p_i \rho_{vac_i}.$$

In sections 3.2 and 3.3 we calculate the elements of the two individual density matrices and in section 3.4 we combine them.

3.2. Radiation Field Coupling. First we will consider the coupling due to the radiation field. Starting with the definitions for the elements of ρ it follows that:

$$(2.42) \qquad \begin{aligned} \rho_{gg} &= c_g c_g^* \\ \dot{\rho}_{gg} &= \dot{c}_g c_g^* + c_g \dot{c}_g^*. \end{aligned}$$

Using equations 2.15 to substitute for $\dot{c}_g$ and $\dot{c}_e$ we find

$$(2.43) \qquad \begin{aligned} \dot{\rho}_{gg} &= \frac{-i\Omega}{2} e^{i\delta t} c_e c_g^* + c_g \frac{i\Omega^*}{2} e^{-i\delta t} c_e^* \\ &= \frac{i}{2} (\Omega^* \tilde{\rho}_{ge} - \Omega \tilde{\rho}_{eg}), \end{aligned}$$

where $\tilde{\rho}_{ge} \equiv \rho_{ge} e^{-i\delta t}$ and $\tilde{\rho}_{eg} \equiv \rho_{eg} e^{i\delta t}$, I will refer to these terms as the complex coherences. In our two-level system if an electron enters the ground state it must have left the excited state. Therefore,

$$(2.44) \qquad \begin{aligned} \dot{\rho}_{ee} &= -\dot{\rho}_{gg} \\ &= \frac{i}{2} (\Omega \tilde{\rho}_{eg} - \Omega^* \tilde{\rho}_{ge}). \end{aligned}$$

We have expressions for the time derivatives of the populations and we now turn our attention to the time derivatives of the complex coherences.

$$\tilde{\rho}_{ge} = \rho_{ge}e^{-i\delta t}$$

$$\dot{\tilde{\rho}}_{ge} = \rho_{ge}\frac{d}{dt}e^{-i\delta t} + \dot{\rho}_{ge}e^{-i\delta t}$$

$$= -i\delta\tilde{\rho}_{ge} + (\dot{c}_g c_e + c_g \dot{c}_e)e^{-i\delta t}$$

$$(2.45) \qquad = -i\delta\tilde{\rho}_{ge} + \frac{i\Omega}{2}(\rho_{gg} - \rho_{ee})$$

By following the same process it is a simple matter to show that:

$$(2.46) \qquad \dot{\tilde{\rho}}_{eg} = i\delta\tilde{\rho}_{eg} + \frac{i\Omega^*}{2}(\rho_{ee} - \rho_{gg}).$$

By comparing equations 2.45 and 2.46 we see that $\dot{\tilde{\rho}}_{ge} = (\dot{\tilde{\rho}}_{eg})^*$.

3.3. Vacuum Field Coupling. To account for the coupling due to the vacuum field, or rather the density matrix terms due to this coupling, we will start just as in equation 2.42 and then substitute using equation 2.38.

$$\dot{\rho}_{ee} = \dot{c}_e c_e^* + c_e \dot{c}_e^*$$

$$= -\frac{\Gamma}{2}c_e c_e^* - c_e\frac{\Gamma}{2}c_e^*$$

$$(2.47) \qquad = -\Gamma\rho_{ee}$$

As a brief aside, equation 2.47 is just a first-order separable differential equation and we can write the solution as:

$$(2.48) \qquad \rho_{ee}(t) = \rho_{ee}(0)e^{-\Gamma t}.$$

Now it is clear that the excited state population decays with a rate of Γ. This justifies the choice of to leave the factor of $1/2$ out of the definition of Γ in equation 2.31. By the same argument as previously

$$(2.49) \qquad \dot{\rho}_{gg} = -\dot{\rho}_{ee} = \Gamma\rho_{ee}.$$

The time derivative $\dot{\tilde{\rho}}_{ge}$ of the vacuum field can as follows:

$$\dot{\rho}_{ge} = \dot{c}_g c_e^* + c_g \dot{c}_e^*$$

$$= 0 - \frac{\Gamma}{2}c_g c_e^*$$

$$(2.50) \qquad = -\frac{\Gamma}{2}\rho_{ge}.$$

The argument that the first term goes to zero is that there is no decay out of the ground state which means $\dot{c}_g = 0$. At first glance this may seem like a contradiction with equation 2.49, however, normalization requires that this be the case. Furthermore, $\dot{\rho}_{gg}$ does not have any dependence on c_e or c_e^*. By a similar argument we find that:

$$(2.51) \qquad \dot{\rho}_{eg} = -\frac{\Gamma}{2}\rho_{eg}.$$

3.4. The Optical Bloch Equations. All that is left to do now is to add the results developed in the previous two sections for the time derivatives of the density matrix elements. This results skipping minor algebraic steps in the coherence equations we find that:

$$\dot{\rho}_{gg} = \Gamma\rho_{ee} + \frac{i}{2}(\Omega^*\tilde{\rho}_{ge} - \Omega\tilde{\rho}_{eg})$$

$$\dot{\rho}_{ee} = -\Gamma\rho_{ee} + \frac{i}{2}(\Omega\tilde{\rho}_{eg} - \Omega^*\tilde{\rho}_{ge})$$

$$\dot{\tilde{\rho}}_{ge} = -\left(\frac{\Gamma}{2} + i\delta\right)\tilde{\rho}_{ge} + \frac{i\Omega}{2}(\rho_{gg} - \rho_{ee})$$

(2.52)
$$\dot{\tilde{\rho}}_{eg} = -\left(\frac{\Gamma}{2} - i\delta\right)\tilde{\rho}_{eg} + \frac{i\Omega^*}{2}(\rho_{ee} - \rho_{gg})$$

These are the Optical Bloch Equations. As a quick sanity consider let's consider the case where we turn off the laser. In this case the radiation contribution to field vanishes and all that remains is the vacuum field. Our equations support this because all of the terms terms related to the coupling with the radiation field go to zero. The only terms that remain are ones due to the interaction with the vacuum field, the only field still present. The converse argument would hold, but is less enlightening since there is no physical way to "turn off" the vacuum field. We now have a set of four differential equations that we can use to solve for any element of the density matrix as a function of time.

4. Saturation and Power Broadening

Our last step before finding an expression for R_{scatt} is to use the Optical Bloch equations, developed in the previous section to solve for ρ_{ee}. In order to simplify the equations we use the population difference $w = \rho_{gg} - \rho_{ee}$, and the fact that relationship that $\tilde{\rho}_{ge} = (\tilde{\rho}_{eg})^*$. To begin, we will rewrite the expression for $\dot{\tilde{\rho}}_{ge}$ using w.

(2.53)
$$\dot{\tilde{\rho}}_{ge} = -\left(\frac{\Gamma}{2} + i\delta\right)\tilde{\rho}_{ge} + \frac{i\Omega}{2}w.$$

Now we need to find an expression for $\dot{w} = \dot{\rho}_{gg} - \dot{\rho}_{ee}$.

$$\dot{w} = \Gamma\rho_{ee} + \frac{i}{2}(\Omega^*\tilde{\rho}_{ge} - \Omega\tilde{\rho}_{eg}) - \left[-\Gamma\rho_{ee} + \frac{i}{2}(\Omega\tilde{\rho}_{eg} - \Omega^*\tilde{\rho}_{ge})\right]$$

(2.54)
$$= 2\Gamma\rho_{ee} + i(\Omega^*\tilde{\rho}_{ge} - \Omega\tilde{\rho}_{eg}).$$

We can move one step further by writing ρ_{ee} in terms of w using the relationship due the normalization that $\rho_{ee} + \rho_{gg} = 1$

$$\rho_{ee} = \rho_{gg} - w$$
$$= 1 - \rho_{ee} - w$$

(2.55)
$$= \frac{1-w}{2}.$$

Plugging this result into equation 2.54 and making use of the relationship between the complex coherences results in:

(2.56)
$$\dot{w} = \Gamma - \Gamma w + i \left[\Omega^* \tilde{\rho}_{ge} - \Omega (\tilde{\rho}_{ge})^* \right].$$

Moving forward we will consider the steady state condition in which $\dot{w} = \dot{\tilde{\rho}}_{ge} = 0$. Our approach now will be to use this condition to set equations 2.53 and 2.56 equal to zero to find a solution for ρ_{ee}. First, we will solve equation 2.53 for w.

$$\left(\frac{\Gamma}{2} + i\delta \right) \tilde{\rho}_{ge} = \frac{i\Omega}{2} w$$

$$\tilde{\rho}_{ge} = \frac{iw\Omega}{\Gamma + 2i\delta}$$

(2.57)
$$(\tilde{\rho}_{ge})^* = \frac{-iw\Omega}{\Gamma - 2i\delta}$$

Now we will use these results in equations 2.54 and solve for W and we find that:

(2.58)
$$w = \frac{\Gamma^2 + 4\delta^2}{\Gamma^2 + 4\delta^2 + 2|\Omega|^2}.$$

We can learn a little more about w by rewriting it as follows:

(2.59)
$$w = \frac{1}{1+s}, \qquad \text{where} \qquad s \equiv \frac{2|\Omega|^2}{\Gamma^2 + 4\delta^2} = \frac{s_0}{1 + \frac{4\delta^2}{\Gamma^2}}.$$

We have now written w as a Lorentzian with saturation parameter s. In the on resonance $(\delta = 0)$ case s reduces to

(2.60)
$$s_0 = \frac{2|\Omega|^2}{\Gamma^2}.$$

Both Γ and $|\Omega|^2$ are proportional to the strength of the radiation field. This suggests that there should be a a way to write s_0 in terms of the the intensity I of the field. This form is experimentally more useful as $I = P/A$, where A is area. So, with a power meter and good of idea of beam waist I can be calculated more easily in an optics lab than Ω or Γ. For reasons I cannot explain the literature does a poor job explicitly showing how this form in terms of I is obtained. So, I have decided to present a simple method I worked out using the previous definitions of Γ and $|\Omega|^2$ in this chapter.

$$\frac{2|\Omega|^2}{\Gamma^2} = \frac{2|\Omega|^2 \tau}{\Gamma}$$

$$= \frac{2E_0^2 \mu^2 \tau}{\hbar^2} \frac{3\pi\epsilon_0 \hbar c^3}{\omega_0^3 \mu^2}$$

(2.61)
$$= \frac{6\pi\epsilon_0 c^3 E_0^2 \tau}{\hbar \omega_0^3}$$

So far all we have done is to introduce $\Gamma = 1/\tau$, plug in the definitions of Ω and Γ, and simplify. Obtaining the final results requires the use of two well know relations:

$$\omega = \frac{2\pi c}{\lambda},$$

and

$$I = \frac{cn\epsilon_0}{2} E_0^2.$$

where n is the refractive index, in a vacuum $n = 1$. Using the first relation to substitute for ω_0 and pulling the proper terms together to replace them with I using the second relations results in:

$$\frac{2|\Omega|^2}{\Gamma^2} = \frac{3\lambda^3 \tau I}{\hbar \pi c}$$

(2.62)
$$= \frac{I}{I_{sat}}, \qquad \text{where} \qquad I_{sat} \equiv \frac{\hbar \pi c}{3\lambda^3 \tau}.$$

We have now defined the saturation intensity I_{sat} which serves as a useful scale for I.

Now we will make use of equation 2.55 to find an expression for ρ_{ee}, which results in:

$$\rho_{ee} = \frac{s}{2(1+s)}$$

$$= \frac{s_0/2}{1 + \frac{s_0}{1 + \frac{4\delta^2}{\Gamma^2}}} \frac{1}{1 + \frac{4\delta^2}{\Gamma^2}}$$

(2.63)
$$= \frac{s_0/2}{1 + \frac{4\delta^2}{\Gamma^2} + s_0}$$

(2.64)
$$= \left(\frac{s_0/2}{1 + s_0}\right)\left(\frac{1}{1 + \frac{4\delta^2}{\Gamma^2(1+s_0)}}\right)$$

Equation 2.64 shows us that ρ_{ee} has a lorentzian line shape withe a line width(FWHM)

(2.65)
$$\Gamma' = \Gamma\sqrt{1 + s_0} = \Gamma\sqrt{1 + \frac{I}{I_{sat}}}.$$

Notice that is the low intensity limit, $I \to 0$ the line width is Γ, but as I increases so does Γ'. This effect is know as power broadening and can be thought of as an example of the time-energy uncertainty principle. In practice equation it is more useful to write ρ_{ee}, using equations 2.63 and 2.62 as:

(2.66)
$$\rho_{ee} = \frac{1}{2} \frac{I/I_{sat}}{1 + (2\delta/\Gamma)^2 + I/I_{sat}}$$

Finally we are ready to write an expression for the scattering rate R_{scatt}. In our two-level model an atoms emit, or scatters photons when they relax back to $|g\rangle$ from $|e\rangle$. Therefore

$$R_{scatt} = \dot{\rho}_{gg}$$

(2.67)
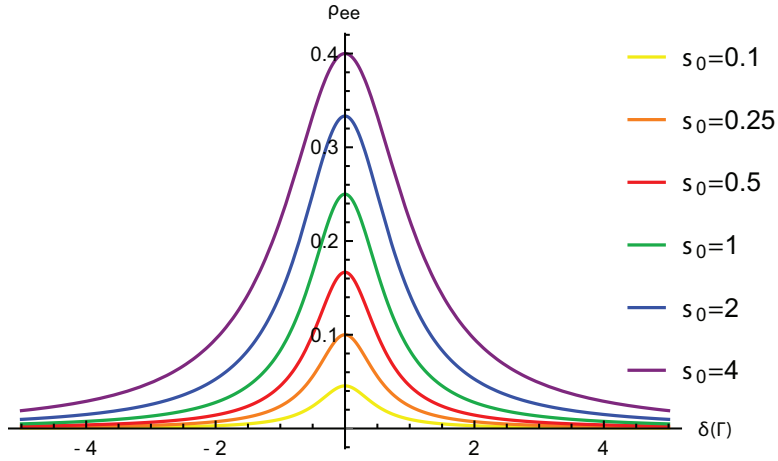$$= \frac{\Gamma}{2} \frac{I/I_{sat}}{1 + (2\delta/\Gamma)^2 + I/I_{sat}}.$$

FIGURE 2.2. Power broadening is illustrated by plotting ρ_{ee} as a function of δ for several different s_0 or I in units of I_{sat}. As s_0 increases the peak on resonance approaches $1/2$ and the Γ' increases.

As I increase, R_{scatt} approaches $\Gamma/2$. This corresponds to individual atoms spending, on average, half their time in the $|g\rangle$ and half in $|e\rangle$. Our definition of I_{sat} is such that $I = I_{sat} \Rightarrow R_{scatt} = \Gamma/4$. In other words when $I = I_{sat}$ half of the maximum number of photons are being scattered.

In the next chapter we will make heavy use of our expression for R_{scatt} as we begin to explore how to achieve the conditions necessary for Bose-Einstein Condensation to occur. There is certainly more that could be said about any of the topics in this chapter. The two-level model we employed turns out to be good model for many situations and is a common tool for solving other questions in atomic physics. The Optical Bloch equations and the density matrix are also commonly used tools the field, and are solved for many different situations. These, however are not critical to description of laser cooling, the first step in achieving Bose-Einstein condensation, which relies on rate at which a laser can deliver momentum kicks to an atom. This is why the approach here has been focused on finding R_{scatt} at the expense of greater breadth.

CHAPTER 3

Laser Cooling

In Ch. 1 we established that a BEC will form given a combination of sufficiently low temperature and high density. If we are going to form a BEC in lab we need to be able to meet these conditions, and doing so experimentally is certainly a nontrivial process. Meeting the first caveat for condensation, achieving $T < T_c$, requires a means by which to cool an ensemble of atoms. The most common way to begin cooling this ensemble is with a technique known as laser cooling, the topic of this chapter. Meeting the second caveat requires a means by which to decrease the volume of the ensemble, if we assume we cannot increase the atom number. This can also be thought of as increasing the spatial confinement of the ensemble, or trapping the atoms more tightly. An initial method for trapping and cooling atoms, called a Magneto-Optical trap (MOT), is described later in this chapter. After a MOT we will rely on a different technique, magnetic trapping, to provide the necessary increase in density and complete the cooling process, which is discussed Ch. 4.

We will begin our discussion of laser cooling with a conceptual description of the technique. Then, for the sake of a more thorough explanation as well as an understanding of the effect of certain experimental parameters we will apply the semi-classical model for atom-light interactions, developed in the previous chapter. Finally we will depart from a general description of laser cooling and describe how it is specifically implemented to cool ^{87}Rb, the species we will use to form our BECs. This theoretical description of laser cooling has been developed from the work presented in [**13, 14, 22**]

1. Qualitative Background

From the advent of spectroscopy light has been used to study matter on a molecular and atomic scale. Usually this work is presented in terms of a conservation of energy, by measuring the energy of photons either emitted or absorbed by an atom it is possible to study its internal structure. However, in addition to energy momentum must also be conserved in atom light interactions. Since photons carry momentum whenever they interact with atoms, through either emission or absorption, there must be a transfer of momentum which means that light can exert a force on atoms. This force provides the basis for laser cooling and trapping techniques developed in the last three decades. Theses tools have in turn lead to many exciting new developments including improved atomic clocks, the study of BECs, and the birth of a new sub-field in Atomic, Molecular, and Optical physics that is making use of these techniques to study what was previously inaccessible. In acknowledgment of their instrumental role in the development on laser cooling and trapping S. Chu, c. Cohen-Tannoudji, and W.D. Phillips were awarded the Nobel Prize in Physics in 1997 [**30, 31, 32**].

Initially, the connection between exerting a force on an ensemble of atoms and cooling it can be difficult to see or may even seem contradictory. However, recalling the Maxwell-Boltzmann speed distribution we can write that:

$$\bar{v} = \sqrt{\frac{8kT}{\pi m}},$$

(3.1)

where $\bar{v}$ is the average speed of a particle in an ideal gas. This tells us that $v \propto \sqrt{T}$ which means that slowing down a group of particles reduces their temperature. This relationship between v and T is precisely the idea that laser cooling is based on. In laser cooling, light from a laser is used to exert a force on an atom that opposes its direction of motion. This slows the atom down which in turn cools it.

The simplest case is to consider an atom of mass m moving in one direction with speed v and a laser beam, with wave number k, propagating in the opposite direction. If the light is on resonance with an allowed transition in the atom it will absorb a photon. This "collision" causes the atom's momentum to decrease by an amount $\hbar k$, the momentum carried by the photon. Using conservation of momentum we can find the corresponding change in the atom's speed, which relates to how much it is cooled as follows:

$$
\begin{aligned}
P_i &= P_f \\
mv_i - \hbar k &= mv_f \\
\Delta v &= -\frac{\hbar k}{m}.
\end{aligned}
$$

(3.2)

After this transition's decay time τ the atom will emit a photon of the same frequency. This again by conservation of momentum will alter the atom's velocity. In the case where a photon is emitted in the same direction that it was absorbed initial reduction in the atom's speed would be completely negated. However, these photons are emitted in a random direction. This means that if we consider the time average of this effect, the change in momentum over many atom-photon interactions, the effect of these emissions cancel each other out, and the net effect is a reduction in the atom's speed which corresponds to a decrease in its temperature. This process is depicted in figure 3.1.
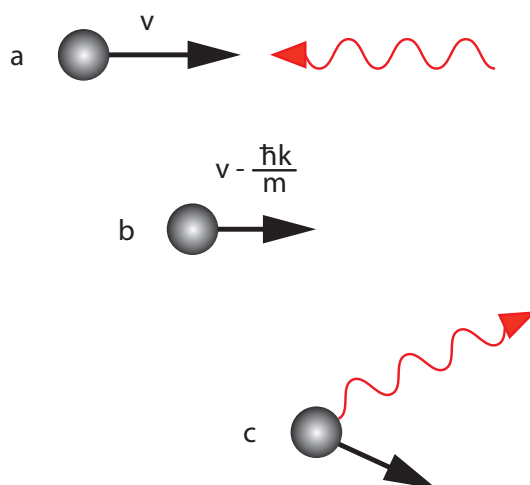

FIGURE 3.1. (a)A resonant photon incident on an atom. (b) The photon is absorbed and the atom feels a momentum kick to the right, causing it to slow down. (c) A photon is spontaneously emitted in a random direction

An initially helpful, albeit, classical analogy is to take a large mass moving is some direction, like a car rolling down a street in neutral. Now take your high velocity ping-pong ball launcher, that you always keep handy, and fire at the car. Each ping-pong ball will reduce the car's momentum by some small, almost negligible, amount but the effect an incredibly large number of collisions will result in a significant decrease in the car's speed.

On its surface we now have a full description of laser cooling. However, upon further inspection many questions have been left unanswered. What does it actually mean for the incident photons to be resonant? What is the briefly mentioned decay time τ? Finally, perhaps most frustrating of all, if there is a change in the atom's momentum then there must be a force exerted on it by the light what is this force? These are all good questions deserving of satisfactory answers.

2. Radiation Force

Building on our work in the precious section we can begin to describe the force exerted on an atom by adsorbing photons $\boldsymbol{F}_{abs}$. For the sake of simplicity we will only concern ourselves with the magnitude F_{abs} as we have already specified that it is directed to oppose the atom's motion. Force can be thought of simply as a change in momentum over time $F = \frac{dP}{dt}$. Every time an atom absorbs a photon it receives a momentum kick of $\Delta P = \hbar k$. So we can write that:

$$(3.3) \qquad F_{abs} = \hbar k \frac{N_{ph}}{\Delta t},$$

where N_{ph} is the number of photons absorbed and δt is the time required to absorb N_{ph}. An excited atom cannot absorb another photon is spontaneously emits, or scatters, a photon to relax back down to the ground state. So an atom can absorb photons at the same rate that it scatters them, meaning that the scattering rate $R_{scatt} = N_{ph}/\Delta t$. This allows that for the slight simplification of equation 3.3 to:

$$(3.4) \qquad F_{abs} = \hbar k R_{scatt}.$$

Now we can make use of equation 2.67, our major result from chapter 2 to write that:

$$(3.5) \qquad F_{abs} = \hbar k \frac{\Gamma}{2} \frac{I/I_{sat}}{1 + (2\delta/\Gamma)^2 + I/I_{sat}}.$$

We now have an expression for the forces exerted on an atom by a laser beam as a function of I and δ. The challenge now is figure our how slow atoms with this force

3. Optical Molasses

Earlier we consider an atom moving against a resonant laser to describe laser cooling. At it core the nature of the interactions in this simple case are the mechanism behind laser cooling. However, with only one laser F_{abs} will only act to slow down the atom when it is moving against the direction of propagation, and will increase its speed, thus heating the system, when it is moving in the direction of propagation. To correct for this we will expand our situation to a one dimensional case in which the atom is free to move in both the positive and negative directions with two lasers, one propagating in each direction. This setup has become known as optical

molasses because the atom is subject a frictional or damping force, which is always acting to slow its motion.

Understanding the premise of optical molasses requires introducing the Doppler effect, which is why it is sometimes referred to as Doppler cooling and was first proposed in 1974 by [33]. If an atom is moving towards a laser it will perceive its frequency to be blue shifted higher and vice versa. This means that a resonant laser in the lab frame will be seen and shift above resonance by an atom moving towards it and below resonance by an atom moving away from it. Our desire is for the net force of the two lasers to be in opposition to the atoms motion. This is accomplished by tuning both lasers below resonance in the lab frame, or red detuning. When an atom moves toward either of the red detuned lasers it will see it as blue shifted closer to resonance and the other as red shifted farther from resonance as shown in figure 3.2. This causes the atom to scatter more photons and feel a stronger force from the laser it is moving towards and to scatter fewer photons from the laser it is moving away from. The net result is to slow the motion of the atom
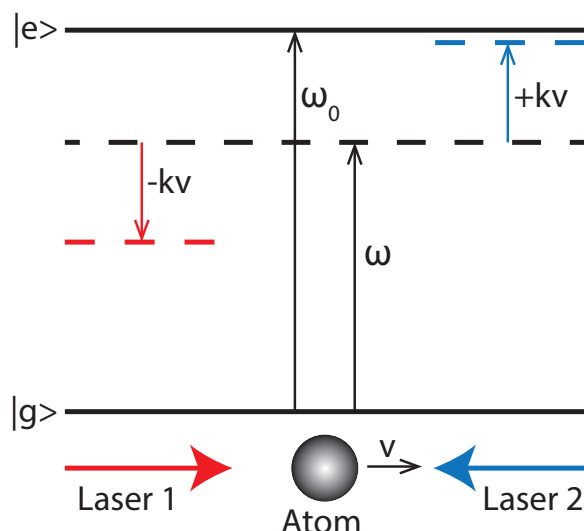
FIGURE 3.2. An atom moving to the right in the radiation fields of two lasers. The lasers are red-detuned from resonance with the $|g\rangle \rightarrow |e\rangle$ transition with frequency ω_0 to a frequency of ω. The atom sees laser 1 further red-detuned away from resonance and laser 2 blue-detuned closer to. Note that the color does not indicated the frequency of the laser but the Doppler shift relative to the atom.

Using this conceptual explanation of the process it is a fairly simple task to describe the net force in the low intensity case. A high intensity model would require considering the dipole force which we will not do here. Before we can use equation 3.5 to write the net force equation of optical molasses we need to redefine the detuning term in order to account for the Doppler effect. It can be rewritten as

$$\delta = (\omega - \omega_0 \pm kv), \tag{3.6}$$

where k is the wave number and v is the speed of the atom. The Doppler shift of laser the atom is moving towards is given by $+kv$ and $-kv$ for the laser the atom is moving away from. Now we can write that

(3.7) $$F_{mol} = F_{abs}(\omega - \omega_0 - kv) - F_{abs}(\omega - \omega_0 + kv).$$

It is reasonable to assume low velocities, $kv \ll \Gamma$, because an atom moving too fast will see the light as Doppler shifted so far from resonance it will not scatter enough photons to be slowed. Under this assumption

$$
\begin{aligned}
F_{mol} &\approx F_{rad}(\omega - \omega_0) - kv\frac{\partial F}{\partial \omega} - F_{rad}(\omega - \omega_0) - kv\frac{\partial F}{\partial \omega} \\
&\approx -2kv\frac{\partial F}{\partial \omega} \\
&\approx 8\hbar k^2 \frac{I}{I_{sat}} \frac{\delta/\Gamma}{[1 + (2\delta/\Gamma)^2]^2} v.
\end{aligned}
$$

(3.8)

Since $I/I_{sat} \ll 1$ it has been dropped from the denominator. Finally we let

(3.9) $$\alpha = -8\hbar k^2 \frac{I}{I_{sat}} \frac{\delta/\Gamma}{[1 + (2\delta/\Gamma)^2]^2},$$

and can say that

(3.10) $$F_{mol} = -\alpha v.$$

In the case where $\delta < 0 \Rightarrow \alpha > 0$ F_{mol} provides a damping force requires that always acts in opposition to an atoms motion. This damping forces makes it as though the atoms are caught in molasses or some other viscous liquid which is where this configuration gets its name and was first implemented by Steven Chu at Bell Laboratories in 1985 [34]. Is is important to note that the detuning must be below resonance in order to cool the atoms, tuning above resonance would result in heating the system. As we have already discussed the system's temperature and energy are related. So, in order to understand the cooling effects of optical molasses it will be more useful to reformulate equation 3.10 to show how F_{mol} reduces the energy of the system. For a particle with energy $E = \frac{1}{2}mv^2$ Newton's second law gives

(3.11) $$\frac{dE}{dt} = Mv\frac{dv}{dt} = vF_{mol} = -\alpha v^2 = -\frac{2\alpha}{M}E.$$

So far we have limited ourselves to the one-dimensional case of one pair counter propagating lasers. Of course in reality an atom is free to move in all three directions. To provide cooling along all three directions optical molasses is usually implemented with three orthogonal pairs of counter propagating lasers. Generalizing for the region of intersection between all six beams is a simple matter of allowing $v^2 = v_x^2 + v_y^2 + v_z^2$, since the behavior in each direction we be like that of the one dimensional case. Unfortunately equation 3.11 cannot be the whole answer because in principle is would allow the energy of the system to go to 0 corresponding with a temperature absolute zero! This is certainly an unphysical result and there must be another, as yet unconsidered, processes occurring to prevent this from happening. Finding the limit of Doppler cooling is the topic of the next section.

4. Doppler Cooling Limit

In this section we will discuss what prevents Doppler cooling from being able to cool a sample to an arbitrarily low temperature. Until now we have consider that the force from one laser beam on atom is $\boldsymbol{F}_{abs}$ which is oversimplification. The force is more appropriately expressed as

$$(3.12) \qquad \boldsymbol{F} = \boldsymbol{F}_{abs} + \delta\boldsymbol{F}_{abs} + \boldsymbol{F}_{spont} + \delta\boldsymbol{F}_{spont}.$$

The affects of $\boldsymbol{F}_{abs}$ have already been take into account in the previous section. As mentioned earlier the time average affect of the spontaneously emitted photons $\bar{\boldsymbol{F}}_{spont} = 0$. We have not yet considered how fluctuations in the absorption and spontaneous emission forces, $\delta\boldsymbol{F}_{abs}$ and $\delta\boldsymbol{F}_{spont}$ impact the net force.

Spontaneous emission always accompanies absorption. Over time it has no net effect, but on a photon by photon basis spontaneous emission leads to a random walk in momentum space because every emission gives a momentum kick in a random direction. This walk is of a number of steps $\mathcal{N}$, equivalent the number of photons emitted. So the mean square velocity increases as

$$(3.13) \qquad \left(\overline{v^2}\right)_{spont} = \mathcal{N}v_r^2 = R_{scatt}t v_r^2,$$

where $v_r = \hbar k/m$ is the recoil velocity imparted on the atom with every emission. In order to consider just one direction at a time, as we did before, the mean square speed along just the z-axis can be written as

$$(3.14) \qquad \left(\overline{v_z^2}\right)_{spont} = \eta R_{scatt}t v_r^2 \qquad \Longrightarrow \qquad \left(\frac{d\overline{v_z^2}}{dt}\right)_{spont} = \eta R_{scatt}v_r^2.$$

Every spontaneously emitted photon gives has a recoil velocity of the z-direction of $v_{rz} = (\hbar k/m)\cos\theta$, the factor of $\eta = \langle\cos^2\theta\rangle$ the angular average has been added to account for this. In the case of isotropic spontaneous emission $\eta = 1/3$.

The fluctuations $\delta\boldsymbol{F}_{spont}$ stem from the fact that an atom does not always scatter the same number of photons in a time t. Fluctuations around the mean scattering rate lead to a walk in mometum spce along the laser beam. Similar to $\left(\overline{v_z^2}\right)_{spont}$ we can write that

$$(3.15) \qquad \left(\overline{v_z^2}\right)_{abs} = R_{scatt}t v_r^2 \qquad \Longrightarrow \qquad \left(\frac{d\overline{v_z^2}}{dt}\right)_{abs} = R_{scatt}v_r^2.$$

So far these results are just for one laser beam. To generalize to describing the atom's motion due to six laser beams in the z-direction requires two assumptions. First, that the scattering rate for a pair of counter propagating beams is $2R_{scatt}$. Second, to account for the contribution of the off axis beams to $\delta\boldsymbol{F}_{spont}$ we will assume that radiation is symmetric so that $\eta = 1/3$ and that each of the 3 pairs contributes equally. The first assumption adds a factor of 2 to both equations 3.14 and 3.15, and the second assumption adds an additional factor of 3 to 3.15. Similar to equation 3.11 we find that

$$(3.16) \qquad \frac{d}{dt}\left(\frac{1}{2}M\overline{v_z^2}\right) = 4E_r R_{scatt} - \alpha\overline{v_z^2},$$

where $E_r = \frac{1}{2}mv_r^2$ is the recoil energy. We now have a result that make physical sense because the additional terms prevents temperature from approaching absolute zero. To determine the steady state condition we set the derivative equal to zero and solve for $\overline{v_z^2}$ and find that

$$(3.17) \qquad \overline{v_z^2} = \frac{4E_r R_{scatt}}{\alpha}.$$

The equipartition theorem tells us that $\frac{1}{2}M\overline{v_z^2} = \frac{1}{2}k_B T$ since the kinetic energy in just the z-direction is one quadratic degree of freedom. To take advantage of this we can multiply equation 3.17 by $\frac{1}{2}M$ so that it equates energies which results in

$$(3.18) \qquad k_B T = \frac{\hbar^2 k^2 R_{scatt}}{\alpha},$$

after also substituting for E_r and v_r. Finally, plugging in for α we find that

$$(3.19) \qquad k_B T = \frac{\hbar \Gamma}{4} \frac{1 + (2\delta/\Gamma)^2}{2\delta/\Gamma}.$$

This is most easily done by first rewriting α as

$$(3.20) \qquad \alpha = -\frac{-4\hbar k^2 \delta}{(\Gamma^2/4 + \delta)} R_{scatt}.$$

Equation 3.19 has a minimum at $\delta = -\Gamma/2$ which corresponds to a temperature of

$$(3.21) \qquad T_D = \frac{\hbar \Gamma}{2k_B}.$$

This temperature T_D is referred to as the Doppler limit and is the lowest possible temperature in an optical molasses of two-level atoms. In practice it turns out that because real atoms are not two-level systems much much colder temperatures are attainable experimentally with Doppler cooling. Cooling below the Doppler limit was first observed in 1992 by W.D. Phillips at NIST [35]. This additional cooling is known as the Sisyphus effect, which is not discussed in this thesis, but was described for the first time by C. Cohen-Tannoudji in the same year [36]. While we now have an effective method to cool atoms it is important to realized that Optical molasses is not a trap. Doppler cooling alone only provides a velocity dependent force and due to the atoms' random walk in momentum space they will eventually leave the region of intersection between all six beams and be lost. The next section describes one technique adding a position dependent force to correct for this.

5. Magneto-Optical Trap

This section describes how a Magneto-Optical trap(MOT) works. The motivation for its development was the desire to confine atoms in an optical molasses by adding a position-dependent force to the existing velocity dependent one and was invented by J. Dalibard and S. Chu 1987 [37] . This is accomplished by turning on a quadrupole magnetic field, usually from a pair of anti-Helmholtz coils, such that the zero of the field and the center of the optical molasses are co-located as shown in figure 3.3. The quadrupole will be discussed in greater detail in Ch. 5 but for now it is sufficient to know that the field is zero at the center of the coils and increases in all direction away from the center. The dangerous misconception that frequently gets developed
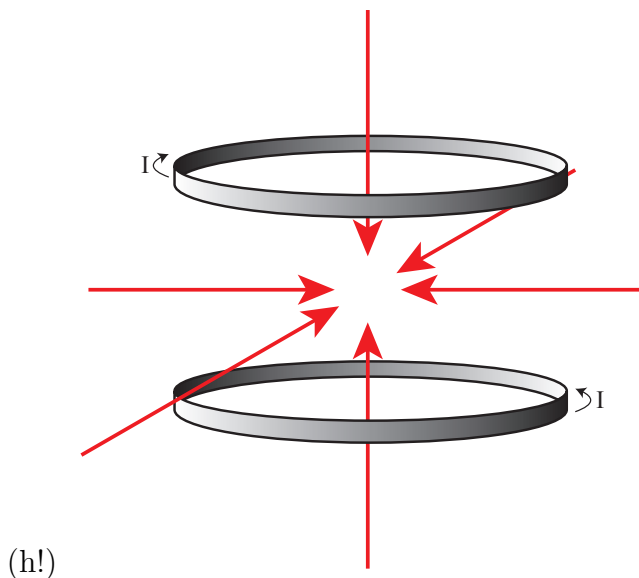
(h!)

FIGURE 3.3. The setup for a MOT. A pair of anti-Helmholtz coils are added along one of the axis of the optical molasses beams.

at this point is that a magnetic force is being used as a position dependent force. This is not the case! The magnetic force does not play a role in this trap as it does in other magnetic traps, described in chapter 5, at least not to any significant level. The position dependent force is due to the Zeeman shift experienced by the atoms as the move away from the center into areas where the magnetic field is non-zero.

When an atom is placed in an external magnetic field the degeneracy associated with projection of angular momentum along the z-axis will be removed due to the Zeeman effect. This is due to a further splitting of the magnetic sub-levels. The splitting for an atom in state $|F, M_F\rangle$ relative to the F energy levels, in the weak-field case, is given by

$$(3.22) \qquad \Delta E_z = \mu_B g_j m_j B_{ext},$$

to a first order approximation. The Bohr magneton is μ_B, and g_j is the Landé g-factor. For the sake of simplicity we will consider an external magnetic field with constant gradient such that in the z-direction $B_{ext_z} = z \frac{dB}{dz}$. As it turns out near the center a quadrupole field this is a very good approximation in any direction. So equation 3.21 becomes

$$(3.23) \qquad \Delta E_z = \mu_B g_j m_j z \frac{dB}{dz}.$$

It is now easy to see that the m_j levels vary linearly as an atom moves away from the center of the trap. For $z > 0$ the $m_j < 0$ levels are Zeeman shifted to lower energy and the $m_j > 0$ are shifted to high energy. This means that the $m_j < 0$ transitions moved closer to resonance and the $m_j > 0$ farther from resonance, since $\delta < 0$ is required for Doppler cooling as shown in figure 3.4. The opposite is true for displacements for $z < 0$ displacements. Using the behavior of the Zeeman shifts as a guide we set the polarization of the pair of beams along the z-axis. The beam propagating in the negative z-direction is set to a σ^- circular polarization, meaning that it has the appropriate polarization to drive $|0, 0\rangle \rightarrow |1, -1\rangle$ transitions. The positive going beam is set to a σ^+ circular polarization so it can drive $|0, 0\rangle \rightarrow |1, 1\rangle$ transitions. This means

that if an moves to a $z > 0$ position it will scatter more photons from the beam propagating in the negative z-direction and feel a force back towards center due to an imbalance in F_{rad} between the two beams. If instead the atom moved to a $z < 0$ position the direction of the would flip and the atom would again be pushed towards the center of the trap. In this way the addition of a magnetic field adds a restoring force in addition to a damping force.
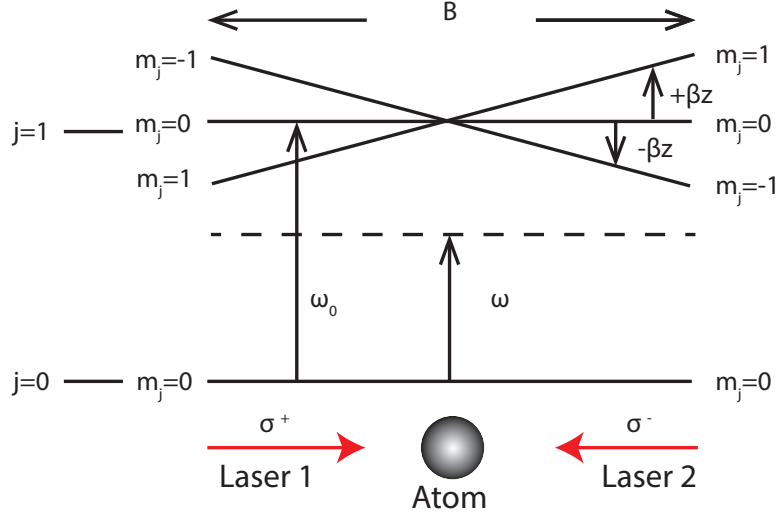

FIGURE 3.4. As an atom moves to areas with $B > 0$ it will scatter more photons from the σ^+ beams and fewer from the σ^- beam. This imbalance in the radiation force will push the atom back towards center. The opposite case occurs for $B < 0$ areas.

We can now incorporate the new Zeeman induced restoring in the optical molasses equations. First, we need to add the Zeeman shifts to the detuning so equation 3.16 becomes

$$(3.24) \qquad \delta = (\omega \pm kv - (\omega_0 \mp \beta z)),$$

where

$$(3.25) \qquad \beta z = \frac{g_j \mu_B}{\hbar} \frac{dB}{dz} z$$

is the Zeeman shift at position z with the approximation of a linear field generalized for any field. Now using the updated δ equation 3.7 can be writen as

$$
\begin{aligned}
(3.26) \qquad F_{MOT} &= F_{scatt}^{\sigma^-}(\omega - kv - (\omega_0 + \beta z)) - F_{scatt}^{\sigma^+}(\omega + kv - (\omega_0 - \beta z)) \\
&= F_{scatt}^{\sigma^-}(\omega - kv - \omega_0 - \beta z) - F_{scatt}^{\sigma^+}(\omega + kv - \omega_0 + \beta z)
\end{aligned}
$$

In addition to assuming $kv \ll \Gamma$ we will aslso assume small displacements from the trap center. So just as before we can approximate F_{MOT} as

$$
\begin{aligned}
F_{MOT} &= -2\frac{\partial F}{\partial \omega} kv - 2\frac{\partial F}{\partial \omega} \beta z \\
(3.27) \qquad &= -\alpha v - \frac{\alpha \beta}{k} z.
\end{aligned}
$$

This shows that for small displacements and speeds a MOT behaves like the classical damped harmonic oscialltor with a damping coeffcient α and spring constant $\frac{\alpha\beta}{k}$. So atoms in a MOT are both slowed and collected at the zero point of the magnetic field.

6. Two-Dimensional Magneto-Optical Trap

A MOT, just like optical molasses, has a maximum capture velocity, only atoms moving sufficiently slow will be trapped which can make initially loading a MOT challenging. The common solution to this problem is to load a MOT from a beam of atoms slowed below the capture velocity directed at its center. The first method for obtaining a slowed beam of atoms is called chirp cooling and involves loading thermal atoms into one of a collimating tube and using a laser propagating in the opposite direction along the tube to slow the atoms. To correct for the Doppler shift of the laser as seen by the atoms decreasing as the atoms slow, the frequency is chirped or ramped down to keep it on resonance. This technique was first implemented by by J.V. Prodan, and W.D. Phillips at NIST in 1984 [**38**]. Coordinating the chirped laser to stay on resonance with many atoms for a long period time proved challenging which prompted W.D. Phillips and H. Metcalf to develop a device called a Zeeman slower later that same year [**39**]. The general theory of operation is that gaseous atoms are loaded into a collimating tube and far red-detuned laser is sent down the tube in the opposite direction. While the atoms are moving very fast down the tube they will see the light red shifted onto resonance and experience a slowing radiation force. A varying magnetic field is applied along the length of the slower so that it is strongest at the end where the laser enters and zero where the atoms enter the tube. This provides a Zeeman shift to keep the atoms on resonance with the laser even after they have been slowed significantly.

While a Zeeman slowers are an effective technique for achieving a slowed beam of atoms, they are large (about one meter long), and require strong magnetic fields. This makes them ill-suited for used aboard the ISS. We will make use of a different method, developed in more recent years, called a 2D MOT, to achieve a slowed beam of atoms [**40, 41**]. In the MOT, or more accurately the 3D MOT, described in the previous section all of the atoms are confined to the center of the trap because that is where the field minimum is located. If instead the field was only quadrupole in two dimensions the field would have a zero along an entire axis. In the two directions where the field increases the atoms experience the same combination cooling and confining force as in a 3D MOT. Along the axis of zero field atoms are unconfined and free to escape. This creates a slowed beam of atoms along the unconfined axis.

This beam can be capped off in one additional direction by adding a red-detuned push beam in the opposite direction on the unconfined axis. The push beam causes atoms to preferentially move in its direction of propagation along the zero line of the magnetic field. The addition of a push beam is indicated by referring to the apparatus as a 2D+ MOT. The + represents the addition of confinement in one direction along the previously completely unconfined axis. A 2D+ MOT can be thought of as taking a full balloon(the 3D MOT) and making a tiny pin hole in it so that gas is allowed to escape in one direction but is still confined in all others. This slowed beam can then be used to load a 3D MOT.

7. Laser Cooling ^{87}Rb

So far our discussion of laser cooling has been limited to a hypothetical two-level atom. Of course in reality when implementing these techniques we are forced to choose a real atom that will not behave as purely a two-level system. The first concern when choosing as atom since our

ultimate goal in to form a BEC is to pick an atom that is bosonic, meaning it has a composite whole integer spin. The next, priority is that the atom have a simple electron structure so that working out a laser scheme for its energy levels is not and experimental disaster. Many isotopes of alkali metals are bosonic making them suitable for laser cooling because they have only one valence electron and the frequencies of these transitions are easily generated by today's lasers. A popular choice that we also use at bates is ^{87}Rb although ^{7}Li, ^{133}Cs, and ^{23}Na among others are also common choices.

Effective laser cooling requires finding what is known as a cycling or closed transition in the hyperfine structure. Such a transition is one that can be driven between a ground hyperfine level and excited hyperfine level that are only allowed to move between each other. The selection rule for electric dipole radiation induced transitions in the hyperfine structure states is that

$$(3.28) \qquad\qquad \Delta F = \pm 1, 0,$$

for an atom in state $|F\rangle$. This result is derived from a conservation of angular momentum between an absorbed or emitted photon and the atom. If we apply this selection rule to the $5^2 P_{1/2} \to 5^2 S_{1/2}$ transition $F' = 3$ can only decay to $F = 2$ as shown in figure 3.5. So we should be able to detune the cooling laser from the $|2\rangle \to |3'\rangle$ transition and drive only those transitions because the light will be far off resonance with other transitions allowed by the selection rules: $|2\rangle \to |1'\rangle$, and $|2\rangle \to |2'\rangle$.

In reality due to the line width of the laser and the Doppler shifting of the moving atoms $|2\rangle \to |2'\rangle$ transitions will occur. Once an atom is in $|2'\rangle$ is it free to decay to $|1\rangle$ at which point it will be lost from the cooling cycle. To get these atoms back into the $|2\rangle \to |3'\rangle$ transition an additional laser, called a repump, tuned to the $|1\rangle \to |2'\rangle$ transition is required. Atoms that have fallen out of cooling cycle will be on resonance with repump and get sent to $|2'\rangle$ where they have a chance to decay down to $|2\rangle$ at which point they reenter the cooling. If instead an atoms decays back to $|1\rangle$ it will simply be kicked back up by the repump. The combination of the cooling and repump lasers allow us to drive transitions in ^{87}Rb almost as if it were a two-level system.
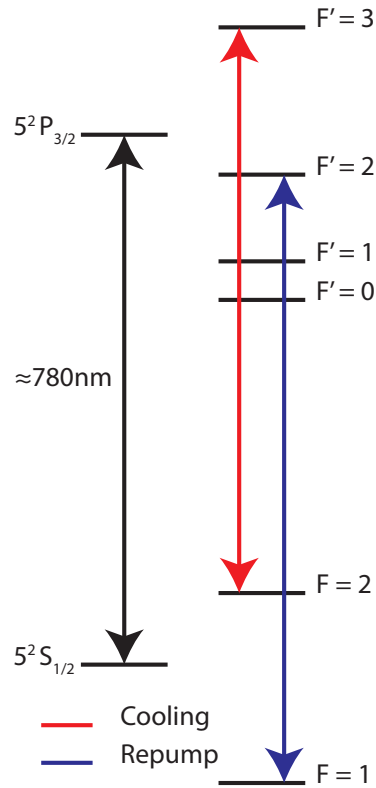
FIGURE 3.5. The cooling light, red-detuned from $|2\rangle \to |3'\rangle$ drives an almost closed transition in ^{87}Rb. The repump, on resonance with $|1\rangle \to |2'\rangle$ returns atoms to the cooling cycle. This figure was drawn using data from [**42**]

CHAPTER 4

Magnetic Trapping

In Ch. 3 three we saw how laser cooling can be used to cool and trap the atoms. Laser cooling allows atoms to start progressing towards condensation, but it is not sufficient due to both the cooling and relatively weak confinement in a MOT. To make it the rest of the way in attaining sufficiently low temperature and high density we will make use of magnetic trapping. Magnetic trapping allows for much tighter confinement leading to high density. Once high density as been achieved in a magnetic trap radio frequency evaporative cooling may be implemented to cool the atoms below T_c. In this chapter we will begin with a theoretical description of magnetic trapping developed from [14, 43, 13]. Then we will move on, to describe a few specific magnetic traps focusing on ones that can be generated on an atom chip that will be used on the experiment at Bates and in the CAL apparatus. Finally we will explain how radio frequency evaporative cooling works.

1. Magnetic Dipole Potential Energy

Magnetic trapping is predicated on the idea that when a magnetic dipole $\boldsymbol{\mu}$ is placed in an external magnetic field $\boldsymbol{B}(\boldsymbol{r})$ it feels a force. Therefore, the dipole will also have an associated potential energy given by

$$V(\boldsymbol{r}) = -\boldsymbol{\mu} \cdot \boldsymbol{B}(\boldsymbol{r}). \tag{4.1}$$

The magnetic dipole moment for an atom in state $|IJFM_F\rangle$ can be written as

$$\boldsymbol{\mu} = -\frac{g_F \mu_B \boldsymbol{F}}{\hbar}. \tag{4.2}$$

This results in such an atom having a magnetic potential energy of

$$V(\boldsymbol{r}) = g_F \mu_B M_F B(\boldsymbol{r}), \tag{4.3}$$

and an associated force of

$$\boldsymbol{F}_{mag} = -\boldsymbol{\nabla} V(\boldsymbol{r}) = -g_F \mu_B M_F \boldsymbol{\nabla} B(\boldsymbol{r}). \tag{4.4}$$

Depending on the orientation of μ when the dipole is placed in the magnetic field, or more accurately when the field is turned on one of two states could arise. When the dipole moment is aligned with the field $\mu_z > 0 \Rightarrow V(\boldsymbol{r}) < 0$ so lower potential energy is attained at higher field. This is said to be the strong field seeking state and an atom occupies it if the product $g_F M_F < 0$. This state cannot be trapped. The trappable state occurs if the dipole moment is anti-aligned with the field, $\mu_z < 0 \Rightarrow V(\boldsymbol{r}) > 0$. Therefore, lower potential is achieved at lower field and $g_F M_F > 0$. So in the trappable state atoms are attracted to field minima thus magnetic trapping becomes simply a challenge of generating a magnetic field with a local minimum. Since

not all states are trappable if the magnetic field is turned on while the sample occupies a variety of M_F levels, those atoms in untrappable states will be accelerated out of the trap and lost. If the Larmor precession given by $\omega_L = \mu B/\hbar$, for atoms initially in trapped states, is greater than the perceived change in direction of $\boldsymbol{B}$ the adiabatic approximation can be applied. This condition is met when $\omega_L \gg \omega_T$ where ω_T is the frequency of oscillation in the trap, or the trap frequency. In this case the atoms move slowly enough that that their dipole moments can follow the field keeping M_F constant. Therefore, as the direction of the field changes an atom will maintain its trapped state. In this case atom's potential energy only depends on $B = |\boldsymbol{B}|$.

2. The Quadrupole Trap

Atoms were first magnetically trapped in a quadrupole field in 1985 at NIST [44]. As mentioned earlier in our discussion of MOTs this field is easily generated by a pair of anti-Helmholtz coils. It meets the local minimum criteria by having $\boldsymbol{B} = 0$ at the center. If we write $\boldsymbol{B} = B_x \hat{\boldsymbol{x}} + B_y \hat{\boldsymbol{y}} + B_z \hat{\boldsymbol{z}}$ the azimuthal symmetry of the field requires that

$$(4.5) \qquad \frac{\partial B_x}{\partial x} = \frac{\partial B_y}{\partial y},$$

where we have chosen the z-direction to be through the center of the coils. Maxwell's Laws state that $\boldsymbol{\nabla} \cdot \boldsymbol{B} = 0$ which requires that

$$(4.6) \qquad 2\frac{\partial B_x}{\partial x} = \frac{\partial B_z}{\partial z}.$$

Using this information to find an expression for the quadruple field we find

$$(4.7) \qquad \boldsymbol{B} = c(x\hat{\boldsymbol{x}} + y\hat{\boldsymbol{y}} - 2z\hat{\boldsymbol{z}}),$$

where c and sets the gradient of the field based on the coil geometry and current. This shows that the field will be linear in all directions and

$$(4.8) \qquad B = |\boldsymbol{B}| = c\sqrt{x^2 + y^2 + 4z^2}.$$

The potential in one direction in a quadrupole trap is shown in blue in 4.1. While the quadrupole trap is useful for its simplicity and ease of implementation, it has a flaw. As trapped atoms cross the the zero point cusp in the potential the adiabatic approximation breaks down. Essentially, the field is changing too rapidly at this point for μ to follow which introduces the possibility for the atom to undergo a ΔM_F transition [45]. If a ΔM_F transition does occur the atom will enter an untrapped state and be lost from the trap. In this case the atom is said to have undergone a Majorana spin flip, as moving from a trapped to untrapped state means that its spin is now pointing in the opposite direction. Atoms lost this way are frequently referred to as Majorana losses. Majorana losses can be avoided by adding a constant bias field to the trap which creates a so-called Ioffe-Pritchard trap. The effect is to both lift the minimum from zero and smooth it out. This can be accomplished by adding one additional coil to the quadrupole trap [46].
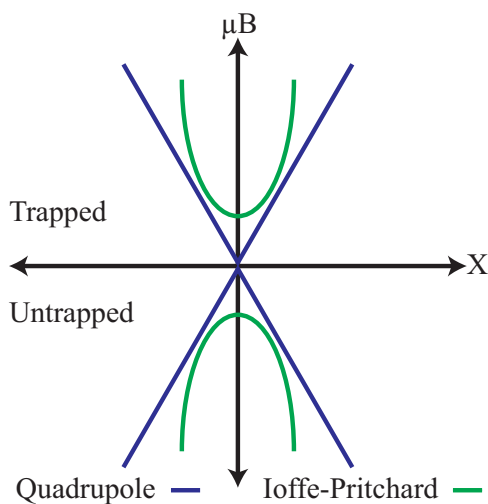
FIGURE 4.1. The trapping potential for the quadrupole and hypothetical Ioffe-Pritchard Trap.

3. Atom Chip Traps

For many years it was common practice for atoms first loaded into a quadrupole trap to then be transferred to other coil based magnetic traps. Over this period a variety of different trap geometries with different coil configurations were developed. The first BEC was formed in an atom chip in 2001 which opened up a whole new set of possibilities for the field[47]. An atom chip is simply a piece of non-conducting material on which conducting traces are printed in order to generate magnetic fields for trapping. The principle behind atom chip-based traps is that the fields from straight conductors are used to form microscopic traps as opposed the much larger traps made using magnet coils. The advantages to atom-chip based magnetic trapping are many, but center around the idea that chip traps offer tighter confinements at much lower currents on a much smaller scale. The tighter confinement allows for more efficient evaporative cooling which leads to faster condensation as colder temperatures. The decreased form factor and power consumption, while a great boon on earth to be sure, are what make it now feasible to put a BEC experiment in the International Space Station. This is why we are specifically concerned with trapping on an atom chip. In this section we will explore a few basic atom chip traps.

3.1. The Infinite Wire Trap. The first example we will consider is strictly speaking a pedagogical example and not an experimentally implementable trap. It does serve to illustrate the basics of atom chip trapping. To begin consider an infinitely long wire carrying a current I. The solution to the Biot-Savart law for this case is

$$(4.9) \qquad\qquad B(z) = \frac{\mu_0 I}{2\pi z},$$

where x is the distance away from the wire and μ_0 is the permeability of free space. If we now add a constant bias field in the negative y-direction, as shown in Figure 4.2, there will be a point directly above the wire where $B_{wire} = B_{y-bias}$. This condition occurs at

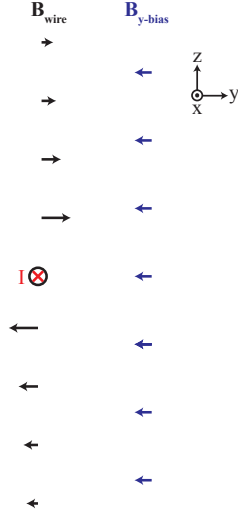$$(4.10) \qquad z_0 = \frac{\mu_0 I}{2\pi B_{y-bias}}.$$

FIGURE 4.2. An infinitely long wire carrying current into the page generates a magnetic field around its self that points in the clockwise direction. A bias field is added in the negative y-direction.

Since at $z = z_0$ B_{wire} and B_{y-bias} are pointing in opposite directions $\boldsymbol{B}(z_0) = \boldsymbol{B}_{wire} + \boldsymbol{B}_{y-bias} = 0$. So atoms in a trappable state in this field will be confined in the x and y-directions, but are free to span the length of the wire. The lack of confinement in the x-direction makes this configuration clearly not a true trap. However, with just a straight wire and constant bias field we have managed achieve magnetic confinement along two axis. This technique of using a constant bias field to cancel a the spatial varying field of a conductor is the basis of atom chip trapping.

3.2. Z-Wire Trap. To add confinement in the z-direction we will simply bend our wire into a z-shape and let it have some finite length as shown in 4.3. If we only bend the wire then we have solved the confinement. A field minimum still occurs at a height z_0 above the center of the middle portion of the z, but now the field increases in either direction along the center of the z as the tails are approached. Therefore, placing the origin in the middle of the z there is a field minimum at point $(0, 0, z_0)$ in all three dimensions, resulting in a trap.
Technically $B_{min} \neq 0$ because the contributions for the the two tails do not completely cancel out at a height z_0 above the wire and this should be an Ioffe-Pritchard trap. Experimentally z_0 is small enough that Majorana spin flips are still an issue. To correct for this we need to increase B_{min} which can be done by adding an additional bias field in the x-direction.
A more rigorous description of the resulting magnetic field can be obtained by applying the Biot-Savart law to each segment of the z and adding the results along with the contributions from the bias fields. The magnetic field of straight wire segment is given by [**26**]

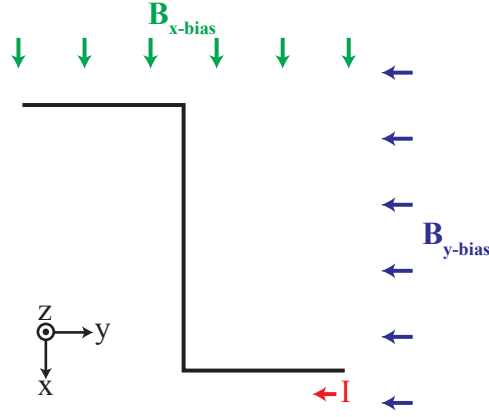$$(4.11) \qquad B = \frac{\mu_0 I}{4\pi s}(\sin\theta_2 - \sin\theta_1),$$

FIGURE 4.3. A z-shaped current carrying wire with constant bias fields in the x and -y-directions. A trap forms centered at a height x_0 above the middle part of the z between the two tails.
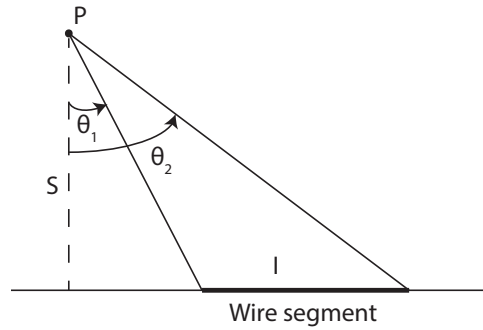

FIGURE 4.4. The magnetic field at point P due to wire segment carrying current I.

where s and θ are defined as shown in Figure 4.4.

As an illustration of the this calculation we will apply equation 4.11 to the tail label 1 in Figure 4.3 which we will say generates a field $\boldsymbol{B}_1$. Keeping the origin at the center of the z and using the coordinate system as defined in Figure 4.3 we can write that

$$(4.12) \qquad s = \sqrt{(x + L_2/2)^2 + z^2},$$

$$(4.13) \qquad \theta_1 = \tan^{-1}\left(\frac{y + L_1}{s}\right),$$

$$(4.14) \qquad \theta_1 = \tan^{-1}\left(\frac{y}{s}\right),$$

where L_1 and L_2 are the lengths of segments 1 and 2 respectively. We will decompose $\boldsymbol{B}_1$ into its components $\boldsymbol{B}_{1x}$ and $\boldsymbol{B}_{1z}$. We will do this by considering the geometry presented in Figure 4.5 and find that

$$(4.15) \qquad\qquad B_{1x} \;=\; -\sin\phi,$$

$$(4.16) \qquad\qquad B_{1z} \;=\; \cos\phi,$$

$$(4.17) \qquad\qquad \phi \;=\; \tan^{-1}\left(\frac{z}{x + L_2/2}\right).$$
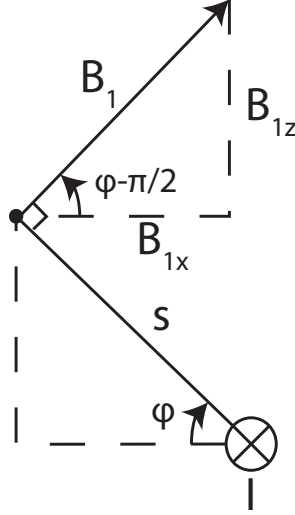
FIGURE 4.5. The direction of $\boldsymbol{B}_1$ facing the negative y-direction for current flowing in the same direction.

A similar process can be made for the other two segments of the z which results in a field with a magnitude of the form

$$(4.18) \qquad B(x,y,z) = \sqrt{(B_{1x} + B_{3x} + B_{x-bias})^2 + (B_{2y} + B_{y-bias})^2 + (B_{1z} + B_{2z} + B_{3z})^2}.$$

Figure 4.6 shows a model of a z-wire trap that could be created on the atom chip at Bates. From this model it is easy to see that z-wire trap offers tight confinement in the y and z-directions, but comparatively weaker confinement in the x-direction. The asymmetry of this trap is undesirable because it leads to less efficient evaporative cooling and condensate that is elongated in one direction. The final atom chip trap that we will investigate offers one method improving the symmetry of the z-wire trap.

3.3. Double Wire Z-Trap. A double wire z-trap can be used to created a dimple trap. This trap is formed by adding two additional wires to the z configuration as shown in Figure 4.8, no additional bias fields are required. The additional wires add to the fields generated by the tails in the region near the center of the z to provide greater confinement. The potential of this trap be calculted in the same manner as before by simply adding in the components in the x and z-directions added by the new wires. This results in a potential of the form

$$(4.19)$$
$$B(x,y,z) = \sqrt{(B_{1x} + B_{3x} + B_{4x} + B_{5x} + B_{x-bias})^2 + (B_{2y} + B_{y-bias})^2 + (B_{1z} + B_{2z} + B_{3z} + B_{4z} + B_{5z})^2},$$
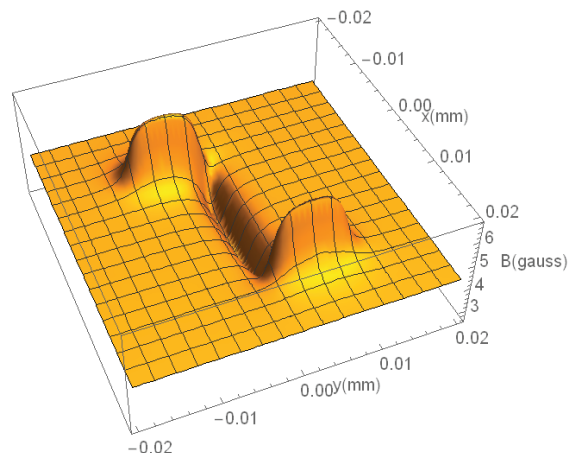
FIGURE 4.6. $B(x, y, z_0)$ is plotted for $I = 2.5A$ for a possible z-wire trap configuration on the atom chip at Bates. For Mathematica code see Lundblad Lab archives.

where the two new wires have been labeled 4 and 5 respectively. Figure **??** models this potential for our chip at Bates for in the x and y-directions for $z = z_0$.
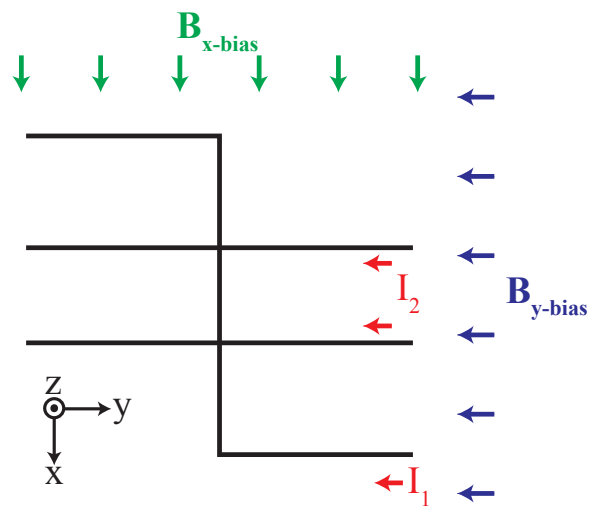

FIGURE 4.7. A double wire z or dimple trap. Additional confinement is achieved by the addition of two dimple wires over the z-wire trap.

4. Radiofrequency Evaporation

Evaporative cooling is the technique implemented in the final stage before condensation occurs. It allows us to reduce the temperature of a sample below T_c. For being an integral process in achieving Bose-Einstein condensation the basic concept is remarkably simple. In general cooling a system requires reducing its energy. Our discussion of laser cooling presented a method for slowing the atoms in a sample to reduce their kinetic energy, and thereby the temperature of the sample. Since each atom carries some energy the total energy of the system can be reduced by simply removing the most energetic atoms. After these atoms are removed, the system will re-equilibrate at a lower temperature, through inter-particle collisions. This
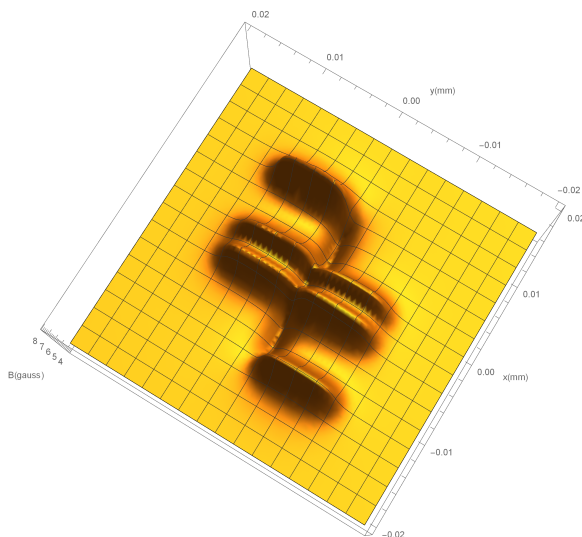
FIGURE 4.8. $B(x, y, z_0)$ is plotted for $I = 2.5A$ and $I = -2A$ for a possible double z-wire trap configuration on the atom chip at Bates. For Mathematica code see Lundblad Lab archives

process is referred to as evaporative cooling and is the mechanism by which a cup of hot coffee cools while sitting on a table. As we all know, this process can be accelerated by blowing across the surface of the coffee to remove the hottest particles faster. This same technique could be used to cool a sample atoms given a method to "blow" the hottest atoms out of the trap.

The trick now is to determine how to evporatively cool magnetically trapped atoms. Since the atoms will be trapped in a vacuum the notion of "blowing" the hottest ones away is not especially helpful because there is no air. So in order to evaporatively the cool our magnetically trapped atoms we need a way to selectively remove the most energetic ones from the trap while still holding onto the cooler ones. Earlier in this chapter we introduced the notion of trapped and untrapped states. Flipping a trapped atom's spin or causing the atom to undergo a $|F, M_F\rangle \to |F, -M_F\rangle$ transition will place it in an untrapped state causing it to be rejected from the trap. So instead of the using electromagnetic radiation to drive transitions between hyperfine levels we can use much lower frequencies to drive transitions between M_F levels. In a harmonic trap the most energetic atoms move the farthest away from the trap center, at the field minimum. In these areas of high field the Zeeman splitting between their M_F levels is the greatest. The energies associated with these transitions are generally on the of kHz to low mHz. So by tuning a radio frequency signal to correspond to a $|F, M_F\rangle \to |F, -M_F\rangle$ transition far away from the trap center and we can couple the M_F and $-M_F$ levels for the hot atoms that make it far from the trap center. Once an atom becomes resonant with this transition it will be moved to the opposite M_F and be removed from the trap as shown in Figure 4.9. By ramping down the frequency atoms with progressively less energy will be removed. If we consider the atoms in the trap to be in a Boltzmann distribution this process removes the high velocity tail of the distribution. After the removal of the atoms a new lower average energy will be established.
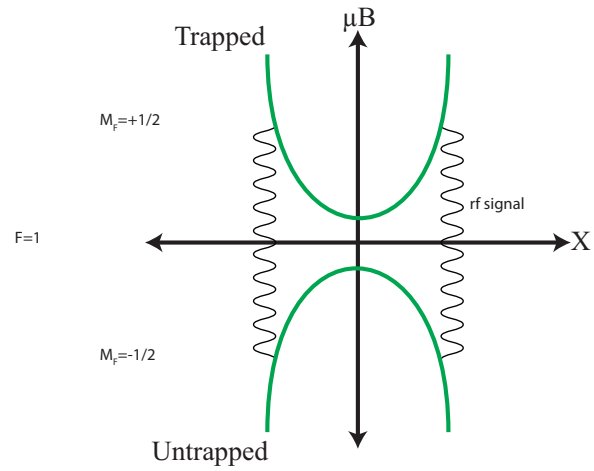
FIGURE 4.9. A rf signal is applied to atoms trapped in a harmonic potential

CHAPTER 5

Experimental Apparatus

In Ch. 1 we explored Bose-Einstein condensation and established BECs as worthy of further study. Then in Ch. 2-4 we presented the techniques of laser cooling and magnetic trapping as means by which to achieve condensation. Therefore, Ch. 1-4 provide answers to questions 1 and 2. Our task now is to answer question 3 by describing how the previously described theory is actually implemented in lab. In this chapter we walk through the experiment and its subsystems that we are building at Bates. Finally, we will complete our answer of question 3 by describing the process by which we will experimentally realize condensation.

1. Vacuum System

The core of the experiment is the RuBECi™ vacuum system, produced by Cold Quanta, as shown in Figure 5.1.
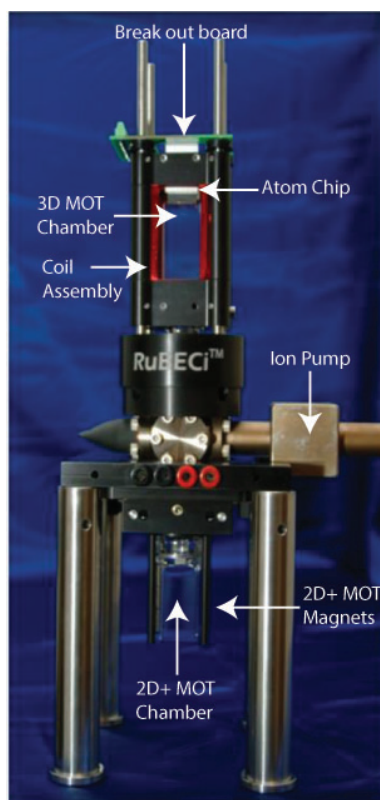
FIGURE 5.1. Cold Quanta's RuBECi™ vacuum system with key components labeled.

The RuBECi™ is a two chamber vacuum system, the 2D MOT if formed in the lower chamber which is then used to load the 3D MOT in the upper chamber. The two chambers are separated

by a silicon disk with a 0.75mm diameter pinhole which allows for differential pumping between the two chambers so that the pressure in the upper chamber can be maintained at 10^{-9} Torr by a 2 l/s ion pump while the vapor pressure in the lower chamber reaches 10^{-7} Torr. This is precisely the advantage of this type of dual chamber vacuum system for BEC creation. It is possible achieve and good ultra-high vacuum in close proximity to the atom source.

The source of ^{87}Rb is a rubidium getter located inside the lower vacuum chamber. Essentially this is just a piece of rubidium salt with a wire running through it. When current is allowed to flow through the salt it heats up and off gas rubidium vapor. This gaseous rubidium is certainly thermal and therefore can be described by a Maxwell velocity distribution. While most of the atoms will be moving too fast to be captured in the 2D+ MOT the distribution requires that there be a low velocity tail of slow atoms which is what the 2D+ MOT is loaded from. We will discuss the optical side of the 2D+ MOT later, but the required two dimensional quadrupole magnetic field is provided by a set of four permanent rare earth magnets located off each of the corners of the 2D+ MOT cell. The slowed beam generated by the 2D+ MOT is aligned through the pinhole and used to load a 3D MOT in the upper vacuum chamber. The coil assembly comprised of four pairs of Helmholtz coils is placed around the upper cell to provide all of the required magnetic fields for the 3D MOT, quadrupole trap, transfer to the atom chip and atom chip traps that are not generated on the atom chip itself. Ultimately the cold cloud of atoms will be loaded into a trap on the atom chip that forms the top wall of the upper chamber. Current is supplied to the atom chip through the break out board which is located directly above the atom chip along with the antenna to antenna to provide and rf signal for evaporative cooling.

By itself the RuBECi$^{\text{TM}}$ provides everything required to make BECs with a few exceptions. The power supplies to provide current to the rubidium getter, coil assembly, and atom chip are separate, but more importantly the RuBECi$^{\text{TM}}$ alone does not provide any of the laser power or optomechanics necessary for laser cooling. The next several sections describe the systems we have built in lab to supply the required laser light.

2. Laser System

This section provides a brief description of the laser systems used before moving on to describe the optics system in detail. The primary cooling light is sourced from a 780nm Vescent diode laser. The laser is locked to the crossover resonance between the $|2\rangle \rightarrow |2'\rangle$ and $|2\rangle \rightarrow |3'\rangle$ of the ^{87}Rb D_2 line using saturated absorption spectroscopy in a vapor cell. This places the laser about 133 MHz red detuned from resonance with the $|2\rangle \rightarrow |3'\rangle$ transition. The repump laser is a home made diode laser built by Prof. Emeritus George Ruff and is locked to resonance with the $|1\rangle \rightarrow |2'\rangle$. This is accomplished by using a beat note technique in which its signal is beat against the master laser to generate an error signal.

3. Optics Switching System

In a typical BEC experiment one laser system provides power to an optomechanical system. The optics then provide the necessary power splitting and polarization control and then deliver the light to the vacuum system to manipulate the atoms as desired. At Bates we have the unusual situation of using the same laser system and partially the same opto-mechanics to provide light to two separate BEC experiments: the original Zeeman slower and large magnetic coil driven experiment (BEC1) and the new 2D MOT and atom chip based experiment (BEC2) that is currently being built. This creates a problem because both control systems need to be able to control some the same shutters and AOMs(Acousto-optic modulator). This section

presents the electronics that we designed and built to allow control of these shared components to be swapped between the two experiments.

Since we only ever intend to run one experiment at a time, solving this issue of splitting control of the shutters is simple matter as they only require a digital control signal. The TTL output from both control systems for a given shutter are used as inputs of a Exclusive OR gate (XOR) and the shutter is controlled directly from the output. Therefore the shutter will open only if one experiment, not both, sends a logic high signal because an XOR has been used instead of an OR gate. This was a desired fail safe feature against human error associated with having both experiments in an active state at the same time.

The sleeping beast really rears its head when working out how to seamlessly swap control of the shared components that require an analog control signal as well as a digital one. In our case components of this type include three AOMs and the lock signal for the master laser. The problem is how to select which set of digital and analog signals to pass through to various components as illustrated in Figure 5.2.
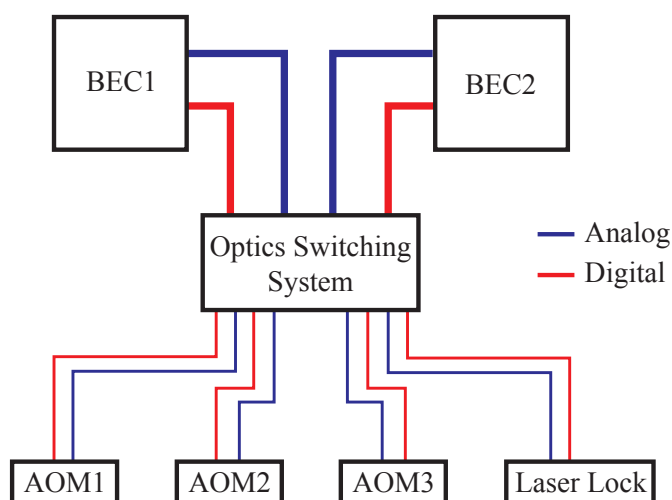

FIGURE 5.2. A Diagram of the analog and digital control signals from each BEC experiment being passed onto the shared components. The optics switching system allows us to select which experiments control signals are used.

It is clear that there is a need for the black box we have dubbed the Optics Switching system to provide the required signal processing. Each BEC control system has four pairs of digital and analog control signals than need to switched between depending on which experiment is running. The question is now what goes inside the black box shown in figure 5.2. The circuit we designed to solve this problem is shown in Figure 5.3. It is worth mentioning that this problem could have solved much more simply with a physical switch or with a dedicated digital out line from one of the control systems. The advantage to the method we have chosen is that the switching occurs automatically, making it one less thing to worry about while running the experiment.

Each of the inputs of the XOR gate marked A and B represent the output from two four input OR gates. These OR gates receive the four digital signals for each of the four components that that require an analog control signal from each experiment's control system. In this way A is high if any of the digital lines from the first experiment are high and B is high if any of the digital lines from the second experiment are high. Moving into the clock circuit the output of
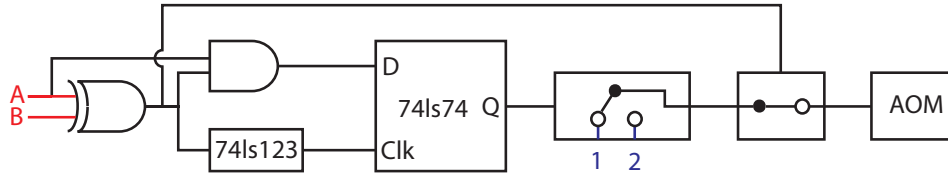
FIGURE 5.3. A schematic of our clock circuit, the electronics that allow the optics switching system to select which analog signal to pass.

the XOR is sent two places the first is an AND gate that is used to discern between when the output of the XOR is high because A is high and B is low or vice versa. Second, the output is sent to a monostable that generates a square pulse every time the output from the XOR goes high. The rising edge from this square pulse is used to trigger the clock on a D-type flip-flop. When the state of the control systems changes so that A is high and B is low the input of the flip-flop D will be high so that when the clock of the flip-flop sees the rising edge from the monostable it will set the output Q high. In the opposite case Q will be set low. The signal on Q is then used to control a digitally actuated single pull double throw switch that moves from connecting the analog signal from BEC1 to the component when A is true and B is false, and the signal from BEC2 when A is false and B is true. Finally, the chosen signal is only passed onto the component if the output of an XOR dedicated that specific component is high, in the same way the shutters are controlled. Table 1 shows the truth table for the clock circuit. The cases where the value of one input changes while the other is high are ignored because only one experiment will be run at a time and when an experiment in inactive all the digital outputs are set to default to low. The critical feature of this circuit is that once control has been switch over to one system, for instance BEC1 it will remain there until it sees a high from BEC2, regardless of how many times the logic level of A changes. This allows the clock circuit to function with just the information provided in the existing digital outputs and does not require an additional dedicated line from either system.

A	B	D	Clk	Q	Switch
↑	F	T	↑	T	1
F	↑	F	↑	F	2
↓	F	F	-	NC	NC
F	↓	F	-	NC	NC

TABLE 1. Truth table describing the operation of the clock circuit.

4. Optomechanics

Now that we have solved the issue of switching control of the optical systems between experiments we will move on to describe the optomechanics for the experiment. Since the layout of optomechanical systems is a fundamentally spatial issue this section is structure around seven figures, each of which illustrates a separate optomechanical subsystem. A brief description of the general purpose and function of each system will be provided, but the finer details will be left in the figures for the reader to study as they wish.

4.1. Master Laser. We will begin all the way upstream with the master laser as shown in Figure 5.4. Approximately 30 mW of power is sent from the master laser to a tapered amplifier that is at driven at about 1850 mA, which results in an output power around 550 mW. From the tapered amplifier beams are split off for spectroscopy and the Zeeman slower in BEC1. The spectroscopy beam is ultimately used to generate the beat note required to lock the repump. After splitting off these two beams the light is double passed through an AOM each time acquiring a shift of +59MHz resulting in light that is approximately 2.5Γ red detuned from resonance with the $|2\rangle \rightarrow |3'\rangle$ where $\Gamma = 6$ MHz and is the line width of D^2 transition. The master laser is used as the cooling light for the MOTs of both experiments. Finally, we select which experiment to send the light to with a flipper mirror. When the mirror is up the light is coupled into a fiber that carries it to BEC1 and when the mirror is down the light is coupled into a fiber going to BEC2.
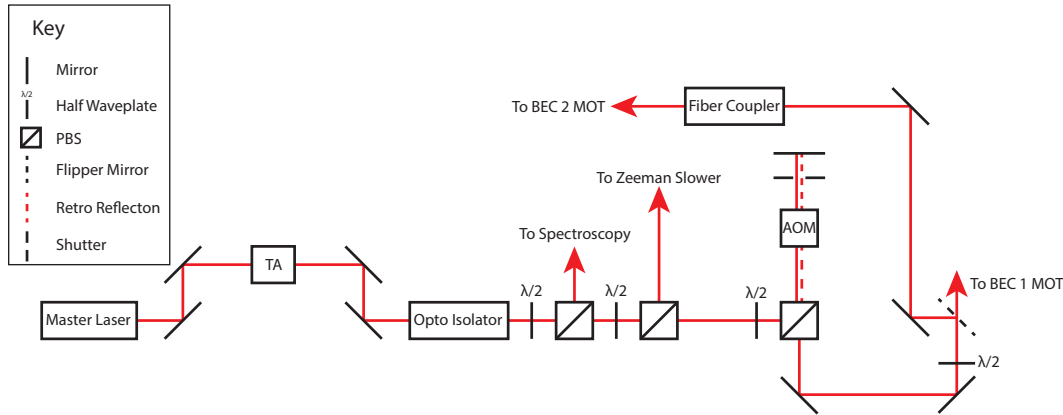

FIGURE 5.4. A diagram of the initial amplification, power splitting, and fiber coupling of the master laser.

4.2. Repump Laser. Now we will describe the analogous system for the repump laser, as shown in Figure 5.5. In a similar configuration the light is amplified by a tapered amplifier usually run at 1550 mA. After this a beam is split off for the Zeeman slower and the rest of the power continues to an AOM where it is shifted almost onto resonance with the $|1\rangle \rightarrow |2'\rangle$ transition. Once again the light is delivered to the chosen experiment by means of a flipper mirror. When the mirror is up the light continues on its original path to be coupled into a fiber going to BEC1's MOT and when the mirror is down the light is coupled into a fiber taking it to BEC2's MOT.

4.3. Master and Repump Combination. As our focus is on BEC2 the the paths to BEC1 will be dropped from our discussion at this point. We will proceed in the case where both flipper mirrors are down and the the master and repump light are both being sent to BEC2. Figure 5.6 shows how the master and repump lights are coupled onto the same path for use in the 2D and 3D MOTs. The output of the trap and repump optical fibers are typically 140 mW and 30 mW respectively. Both lights are combined on a polarizing beam splitter (PBS). Instead of the throwing the rejected light away we chose to use it for the push beam in the 2D+ MOT. Finally another PBS is used to split the combined trap light into beams for the 2D and 3D MOTs.
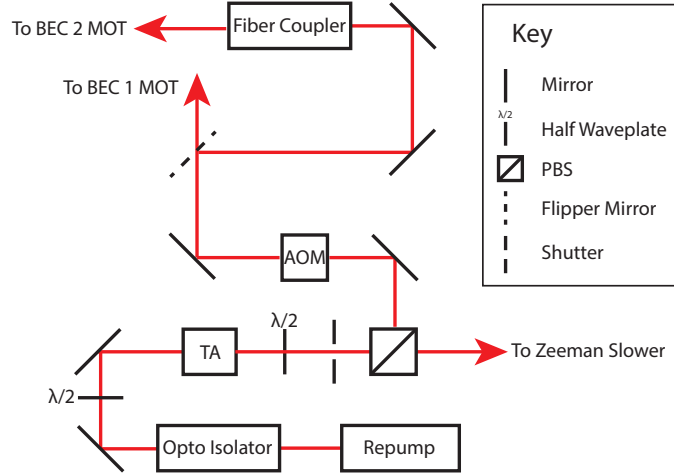
FIGURE 5.5. A diagram of the initial amplification, power splitting, and fiber coupling of the repump laser.
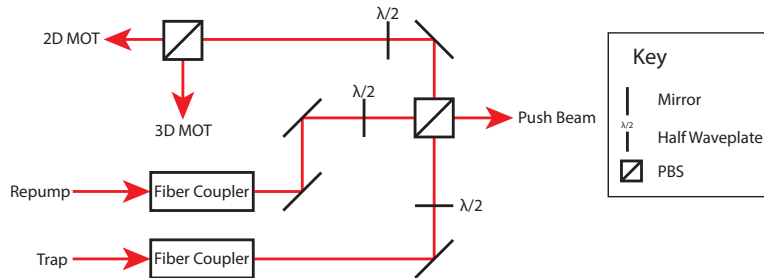

FIGURE 5.6. The output of the master and repump fibers are coupled onto the same path for future use in the 2D and 3D MOTs.

4.4. 2D MOT. We will now follow the 2D MOT beam paths as shown in Figure 5.7. The first step is to send the beam into a periscope to raise it to a height of 3.75 in above the optical table from an initial height of 2.00 in. This aligns the beams appropriately with the lower vacuum cell. Once at this raised height the beam is split into two beams each with about 27 mW of power from the master laser and 3 mW from the repump. Both beams are then expanded in cylindrical telescopes to provide beams with a horizontal beam waist of (10.8 ± 0.4) mm and vertical waist of (20.2 ± 0.6) mm. From here the beams are directed into the lower vacuum cell. The counter propagating beams required to form a MOT are attained by retroreflecting the beams back on themselves. Quarter waveplates are used before both beams enter the vacuum chamber in order to ensure the circular polarization required for a MOT as described in Ch. 3. The analysis required to align these waveplates will be discussed in the next section.

The beam waists were measured by incrementally blocking the beam with a razor blade and measuring the power of the that was not blocked. These data, a set of points of power as a function of distance the edge of the razor had been extended, were fit to a gaussian error function. Figure 5.8 shows an example of this fit.

To have a 2D+ MOT with additional confinement along one direction of the unconfined axis a push beam is required. The challenge is that the push beam must be directed vertical up into the lower vacuum chamber in order to improve loading into the 3D MOT as shown in Figure 5.9. The height of the push beam is lowered in a periscope to 1.30 in above the table so that it
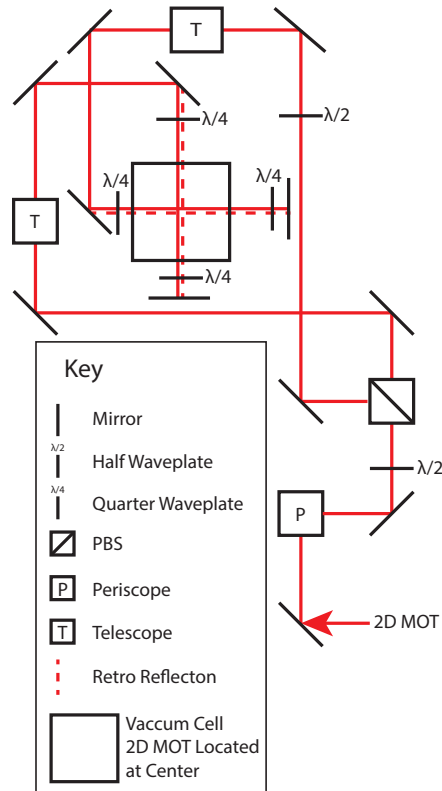
FIGURE 5.7. After being raised 3.75 in off the table the 2D MOT beams are split in two and expanded in a telescope. These beams are directed into the lower vacuum cell and retroreflected to provide the required master and repump light for a 2D MOT.
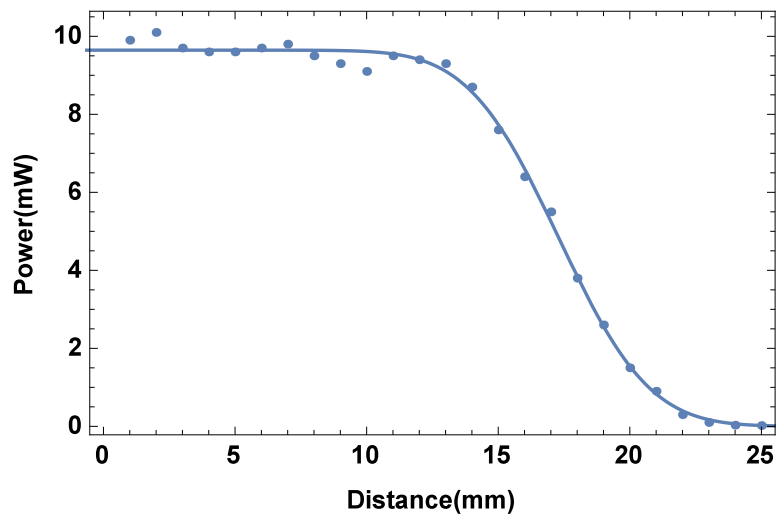

FIGURE 5.8. A plot of 2D MOT horizontal beam waist data and the Gaussian error function fit. For Mathematica code see Lundblad Lab archives.

can get underneath the lower vacuum chamber. It is also expanded in a telescope to maximize the portion of the experiment's bore that it covers. Once the push beam reaches the vacuum

chamber a ccd camera is coupled onto its path using a PBS to image the 2D MOT from below. The path is then directed vertically up in to the vacuum chamber by means a 45^0 angled mirror.
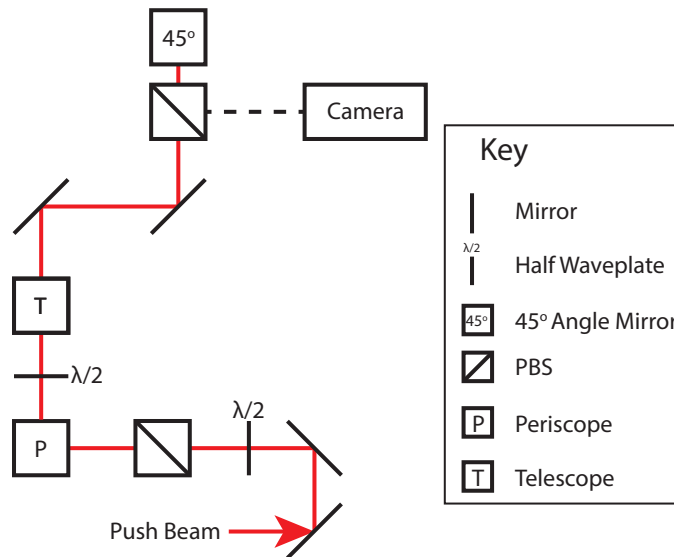

FIGURE 5.9. Diagram of the push beam's path to the vaccum chamber. A ccd camera is coupled onto the push beam path on the last PBS to image the 2D MOT from below.

4.5. 3D MOT. The only parts of the experiment's optomechanical system left to be discussed are the power splitting and polarization control for the 3D MOT. After being separated from the 2D MOT beam the 3D beam is further divided into four beams each of which is then symmetrically expanded in telescopes and carry about 26 mW of power, as shown if Figure 5.10.
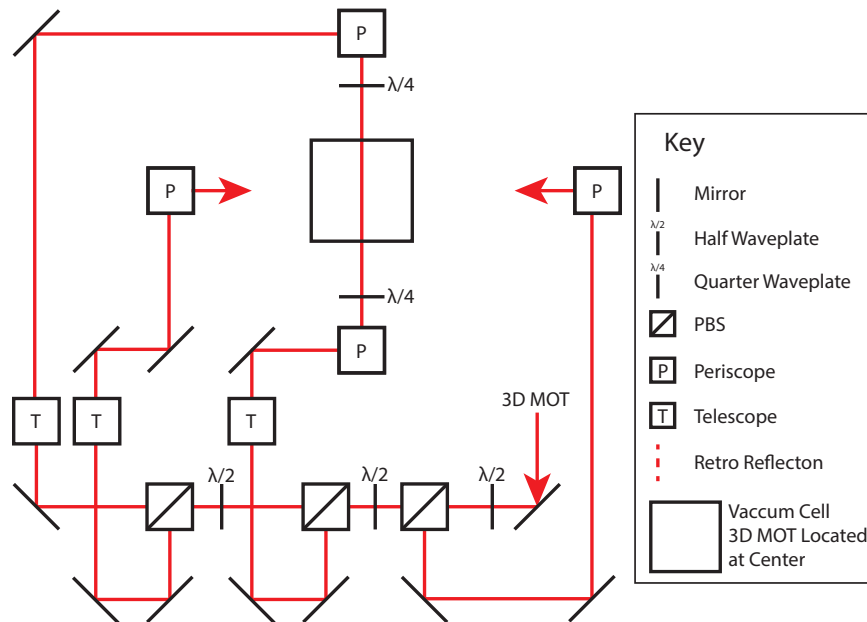

FIGURE 5.10. A diagram of the power splitting, expansion, and polarization control of the 3D MOT beams.

After the telescopes two beams are lifted in periscopes to the appropriate height and directed into the upper vacuum chamber after having their polarization set by quarter waveplates. The other two 3D MOT beams are lifted in periscopes to point below the center of the vacuum chamber to send the beams at angle through the center of the cell as shown in Figure 5.11. These beams are separated by 45^0 and are retroreflected. So this 3D MOT is formed using four beams two of which are retroreflected to reach the required total of three pairs of counter propagating beams.
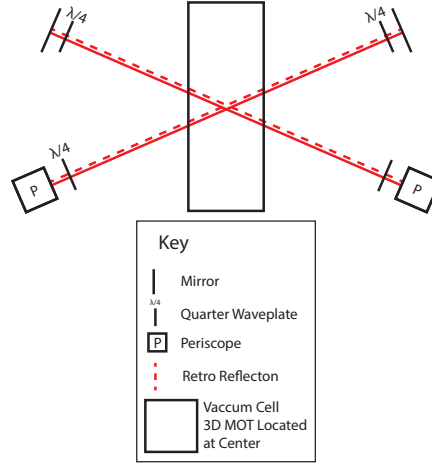

FIGURE 5.11. Two of the 3D MOT beams are sent on angles through the vacuum chamber so that the are separated by 45^0.

5. Polarization Analysis

As mentioned earlier it is not sufficient for the laser beams in a MOT to be detuned from resonance with the cooling transition. In order to conserve angular momentum the selection rules require that the light must be circularly polarized light to drive to desired atomic transitions. In this section we will describe how quarter waveplates are used to turn linearly polarized into circularly polarized for use in laser cooling. To do this we will begin by formally introducing the concept of polarization, a concept which as of yet I have judiciously danced around actually defining. To do this we will loosely follow the presentation in [**48**].

In classical electromagnetic theory the typical picture of an electromagnetic wave is that of a magnetic and electric field whose amplitudes vary sinusoidally and orthogonal to each other, that copropagate as transverse waves. Usually, the assumption is made that the orientation of the fields with respect the direction of propagation stays constant, but in general there is no reason why this must be the case. In fact, in the case of naturally occurring light it is not the case at all, this orientation or polarization as it is more commonly called, changes rapidly. Polarization is how the direction of the electric and magnetic fields relative to the direction of propagation, the question is now mathematically describing the polarization. Since the directions of the electric and magnetic fields obey the right hand rule, one implies the other so we need only consider the direction of one to the describe the polarization. The convention in optics is to use the direction of the electric field $\boldsymbol{E}$ as the direction of polarization. In general we can write that

$$(5.1) \qquad \boldsymbol{E} = E_0 e^{i(\boldsymbol{k}\cdot\boldsymbol{r}-\omega t+\phi)}\hat{\boldsymbol{p}},$$

where E_0 is the amplitude of the field, $\boldsymbol{k}$ is the wave vector, ω is the angular frequency of oscillation, ϕ is some constant phase shift, and $\hat{\boldsymbol{p}}$ is the direction of polarization. If we choose z to be the direction of propagation $\boldsymbol{E}$ can easily be written as

$$(5.2) \qquad \boldsymbol{E} = E_{0x}e^{i(kz-\omega t+\phi_x)}\hat{\boldsymbol{x}} + E_{0y}e^{i(kz-\omega t+\phi_y)}\hat{\boldsymbol{y}},$$

or in terms of complex amplitudes as

$$(5.3) \qquad \boldsymbol{E} = \tilde{E}_{0x}e^{i\phi_x}\hat{\boldsymbol{x}} + \tilde{E}_{0y}e^{i\phi_y}\hat{\boldsymbol{y}}.$$

This form lends itself well being described using linear algebra, and to do this we will put $\boldsymbol{E}$ in the form

$$(5.4) \qquad \boldsymbol{E} = \begin{bmatrix} \tilde{E}_{0x}e^{i\phi_x} \\ \tilde{E}_{0y}e^{i\phi_y} \end{bmatrix},$$

which is known as the Jones vector. The convention is to normalize Jones vectors so that they just represent the direction of polarization For example, the Jones vectors describing linearly polarized light with respect to the x and y-directions are

$$(5.5) \qquad \begin{bmatrix} 1 \\ 0 \end{bmatrix}, \text{ and } \begin{bmatrix} 0 \\ 1 \end{bmatrix}$$

respectively.

Nonlinearly polarized light is obtained when the phase difference between the components of the Jones vector is nonzero, $\phi_y - \phi_x \neq 0$. More specifically, circularly polarized occurs when one component lags the other by $\pi/2$ radians, $\phi_y - \phi_x = \pm\pi/2$. The result of this is that the trailing component attains the same value as the leading component at a time $\omega\pi/2$ later resulting in the direction of polarization rotating circularly in time. The Jones vectors describing left and right hand circularly polarized light are

$$(5.6) \qquad \frac{1}{\sqrt{2}}\begin{bmatrix} 1 \\ i \end{bmatrix}, \text{ and } \frac{1}{\sqrt{2}}\begin{bmatrix} 1 \\ -i \end{bmatrix},$$

where left and right refer counterclockwise and clockwise rotation. So, circularly polarized light can be created by making the phase difference between the components of the Jones vector $\pm\pi/2$. In linear light where there is no phase difference this can be accomplished by introducing a phase shift of $\pm\pi/2$. Fortunately this is a solved problem, the quarter-wave plate is a device that is designed to alter the phase difference by $\pm\pi/2$. This is accomplished by cutting a sheet of a birefringent material so that the axes of minimum and maximum refraction are perpendicular and the difference in their optical depths is one quarter of the wavelength it is intended to manipulate. This is certainly a brief description of the quarter-wave plates, but a more detailed exploration is beyond the scope of the this thesis, greater detail can be found in [**48**]. For achieving our ultimate goal of laser cooling we interested in using quarter-wave plates as a tool which makes it sufficient to understand what a quarter-wave plate does if not precisely how it works.

The true power of writing the direction of polarization as a Jones vector is that any optical element that manipulates polarization can be described by an operator called a Jones matrix. To find the effect a given element has on light of a certain polarization we simply apply the

element's Jones matrix to the Jones vector for the light incident on the element. The resulting Jones vector describes the transmitted light's polarization state after the optical element has acted on it. The Jones matrix for a quarter-wave plate with its fast axis oriented vertically is

$$(5.7) \qquad \begin{bmatrix} 1 & 0 \\ 0 & -i \end{bmatrix}.$$

If we shine light that is linearly polarized at 45° to the axis through such a quarter- wave plate the resulting polarization is given by

$$(5.8) \qquad \begin{bmatrix} 1 & 0 \\ 0 & -i \end{bmatrix} \frac{1}{\sqrt{2}} \begin{bmatrix} 1 \\ 1 \end{bmatrix} = \frac{1}{\sqrt{2}} \begin{bmatrix} 1 \\ -i \end{bmatrix},$$

which is right hand circularly polarized. Generalizing from this specific example, circularly polarized light can be obtained by passing linearly polarized light through a quarter-wave plate oriented such that the angle between the fast axis and the direction of polarization is 45°. By passing our laser cooling light through polarizing beam splitters that transmit only vertically linear polarized light and reflect only horizontally linear polarized light we are able to truly work with the case shown in equation 5.8. The only challenge left to circularly polarize light in lab is determining the appropriate orientation of a quarter-wave plate. This can be done by using a polarization analyzer which is simply a quarter-wave plate that has been set to turn incident circularly polarized light into either vertical or horizontally polarized light, and a polarizing beam splitter. Precisely which circular polarization is linearly polarized with respect to which axis depends on the specifics of a how a given analyzer is set, and for our purposes is not important.

The experiment used to determine the orientations of a quarter-wave plate that result in the circular polarization of vertically or horizontally polarized light is shown in Figure 5.12.
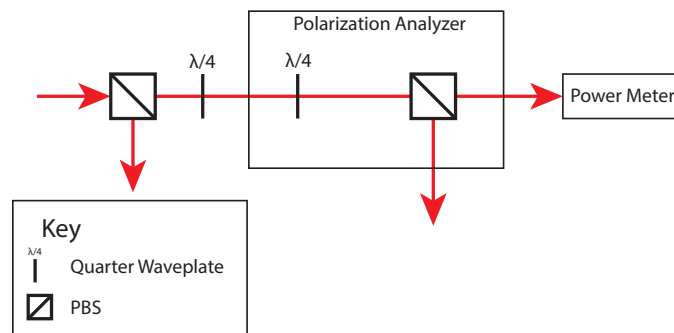

FIGURE 5.12. The optical experiment used to determine which orientations of the quarter-wave plate produce circular polarized light from incident linearly polarized light with respect to the vertical or horizontal axes.

The beam in first sent through a PBS in order to ensure a pure linear polarization state, and the reflected mode of the PBS is discarded. The light is then incident on the quarter-wave that is being calibrated and then continues into the polarization analyzer. When the quarter-wave plate is adjusted such that that it produces circularly polarized light the quarter-wave plate in the analyzer will then reconvert it to linearly polarized light. In this case the final PBS will either transmit or reflect all of the light causing the power meter to read a maximum or a minimum. So in a plot of power versus orientation of quarter-wave plate being calibrated the

extrema represent the orientations that result in circularly polarized light. Figure 5.13 is an example of one such plot for one of the quarter-wave plates used in the 3D MOT. Maxima occur at $(74.6 \pm 0.3)°$ and $(254.6 \pm 0.3)°$, and minima occur at $(164.6 \pm 0.3)°$ and $(344.6 \pm 0.3)°$ based on fitting the data to a function of the form

(5.9)
$$P(\theta) = P_0 \cos^2\left(\theta \frac{\pi}{180} + \delta\right),$$

where θ represents the orientation of the wave plate in degrees, P_0 is the maximum power and δ is some constant phase shift. The uncertainties represent two standard deviations and are obtained through standard propagation of error.
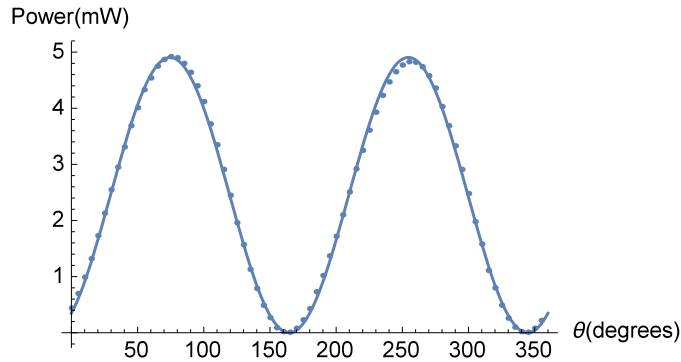

FIGURE 5.13. A plot of power as function of orientation for one full rotation of a quarter-wave plate used in the 3D MOT.

The fact that two maxima and two minima are observed is expected because for one full rotation of the quarter-wave plate there will be two possible orientations of the fast axes that place it at a 45° angle with respect to the direction of polarization and two that place it at a −45° angle.

By conducting a similar analysis for all of the quarter-wave plates intended to be used in the MOTs we are able to ensure proper polarization. The ambiguity of not knowing which extrema correspond to which direction of circular polarization is not critical to resolve in an experimental context. The orientation of the quarter-wave plates on the retro reflected beams does not matter. Since permanent magnets are used for the the 2D MOT magnetic field the directions of its required polarizations are fixed. However, it is a simple matter to test the four possible combinations of wave plate orientations while looking for a MOT. For a 3D MOT, based on the direction of the field lines we can deduce that the polarization of the beams coaxial with the magnet coils must be opposite that of the other beams. So, if the first guess of polarizations is wrong it is a simple matter to reverse the direction of the current through the coils thereby reversing the direction of the field or to flip all of the quarter waveplates.

6. Coil Assembly

Now that we have laser power of the correct polarization delivered to the proper locations it is necessary to consider how the required magnetic fields for the 3D MOT and magnetic trapping will be generated. All of the necessary fields not from the atom chip will be generated using magnet coils in the coil assembly which fits around the upper vacuum cell as shown in Figure 5.1. The coil assembly contains four pairs of coils one in each Cartesian direction x, y, and z plus an additional pair of transfer coils [49]. The x coils can be used in either a Helmholtz or

anti-Helmholtz configuration. The anti-Helmoholtz configuration provides the quadrupole field for the both the 3D MOT and quadrupole trap and the Helmholtz configuration will provide one of the bias fields for trapping on the atom chip. The coils in the y and z coils will be used to provide the bias fields for the trapping on the chip and to cancel out any stray background magnetic fields. The final set of coils are the transfer coils which are oriented in the x-direction, but are offset from the x coils so that their center is closer to the atom chip. These coils will be used to help transfer the atoms from the quadrupole trap to the atom chip.

7. Control System

Now that we have discussed all the various subsystems required to form a BEC in this experiment the final piece of the puzzle is an automated control system to coordinate all of the moving parts. We have chosen to use a program called LabScript which is a python based control system designed for shot experiments. The advantages to LabScript over other control systems are many. First programming a shot in LabScript is very simple. Each command that must be executed by some part of the experiment during a shot is accomplished by one line of code in the control sequence. The clock for a given shot is started when the first command is issued and the previous commands are executed some specified periods of time later. A nice feature of LabScript is that the time for a for a command to issued can given relative to the previous command so it is not necessary to track the total duration of the control sequence while programming. In a BEC experiment a shot generally ends by imaging the condensate. Frequently the analysis of these images must be handled by another program because other control systems do not have the functionality to run the analysis themselves. Since LabScript is Python based, which is a fully functioning high level programming language, it has the capability to do all of the required analysis itself which eliminates the need for a separate analysis program. Finally LabScript is text based, which allows for much cleaner better organized code as compared to other graphically programmed control systems frequently used in laboratories.

8. Process to Realize a BEC

In this last section we will discuss process by which we will form a BEC. A shot begins by using the 2D+ MOT to load a 3D MOT. After the 3D MOT has reached its maximum capacity the magnetic field is turned off to allow for a brief period of sub-Doppler cooling in optical molasses. The next step is to optically pump the atoms into the the $|2, 2\rangle$ state. While the $|2, 1\rangle$ state is also magnetically trappable using the $M_F = 2$ as opposed to $M_F = 1$ results in magnetic trapping force that is a factor of 2 stronger which greatly improves trapping. After the optical pumping phase all of the lasers are shuttered and the x coils are ramped up to load a quadrupole trap. This marks the end of the laser cooling part of the process and the beginning of the magnetic trapping phase. Once in the quadrupole trap the atoms are slowly moved closer to the atom chip by using the transfer coils to slowly shift the zero point of the field closer to the surface of the chip. When the atoms are close enough they are loaded onto the atom chip by ramping up a chip trap. With the atoms trapped on the chip the final stage is to evaporatively cool the sample to below T_c at which point condensation occurs. Finally, a measurement of the resulting BEC can be made using resonance imaging. For a more detailed description of BEC production on a similar system the reader is directed to [50].

CHAPTER 6

Conclusion

We have now answered the three questions that were posed in the introduction. With regard to question 1 (Ch. 1) a BEC forms when bosons rapidly condense into the ground state because the system has become sufficiently cold and dense. BECs are macroscopically large systems that behave quantum mechanically which is why they are of great use in the study of quantum mechanics, solid state physics, and the development of high precision measurement techniques. To answer question 2 (Ch. 2-4) we provided a theoretical description of how to take thermal atoms to the point of condensation, $T < T_c$. This process begins with laser cooling to initially cool and trap the atoms. From a MOT atoms are loaded into a magnetic trap which allows for increased density and further cooling from radiofrequency evaporation. One of many possible answers to question 3 (Ch. 5) is provided with a description of the systems we have built in lab over that past two semesters. In general laser cooling requires the locking of lasers to specific frequencies in order obtain the proper detuning, power splitting to create the 3 pairs of counterpropagating beams required for a MOT and optical molasses, and finally polarization control in order to drive the appropriate atomic transitions in a MOT. Our experiment uses a 2D+ MOT formed in the lower chamber from vapor pressure, to load a 3D MOT in the upper chamber. Magnetic trapping for this kind of atom chip experiment follows a two-fold scheme. First, atoms are magnetically trapped in a standard quadrupole field generated by a pair of anti-Helmholtz coils. The atoms are then transferred from the quadrupole trap to the atom chip with the help of an additional pair of so-called transfer anti-Helmholtz coils. Once the atoms are loaded onto the atom chip condensation is achieved through radiofrequency evaporation. Question 3 is lacking a more experimentally detailed answer because we ran into several setbacks over the course of the year. I would like to take the time to briefly describe these challenges and present the qualitative results we have for the 2D MOT.

The original plan was that during the first semester we would build the optics switching system while waiting for the first batch of optomechanical parts to be machined with the goal of loading a 3D MOT by the end of the semester. Designing and assembling the switching electronics went more or less smoothly and the system was successfully integrated with the existing experiment's control system. Unfortunately, due to other demands on machine shop time the optomechanical parts for the 2D+ MOT were not ready until the beginning of the second semester. At the start of the spring semester we were able to move forward aligning optics and begin looking for the 2D+ MOT. We spent the next two weeks searching, unsuccessfully, for a MOT only to finally discover that the ion pump had failed. After receiving a new pump from ColdQuanta we found a 2D MOT in a matter of minutes after the Rb getter had warmed up, as shown by the bright spot in Figure 6.1. The images were taken using a CCD camera with a 33.5 mm convex lens approximately 5 cm in front of the camera looking up into the vacuum chamber by using a 45° mirror placed directly under the lower chamber. The bright region in the upper left corner of both images is just scattered light from the 2D MOT beams. The ring in both images is the window into the lower vacuum chamber to provide optical access for the push beam from below, and the gray haze within the ring is repump enhanced florescence of

the rubidium vapor from the getter. The bright spot present in the image on the left is the 2D MOT. No MOT is present in the image on the right, which is presented for the purpose of comparison.
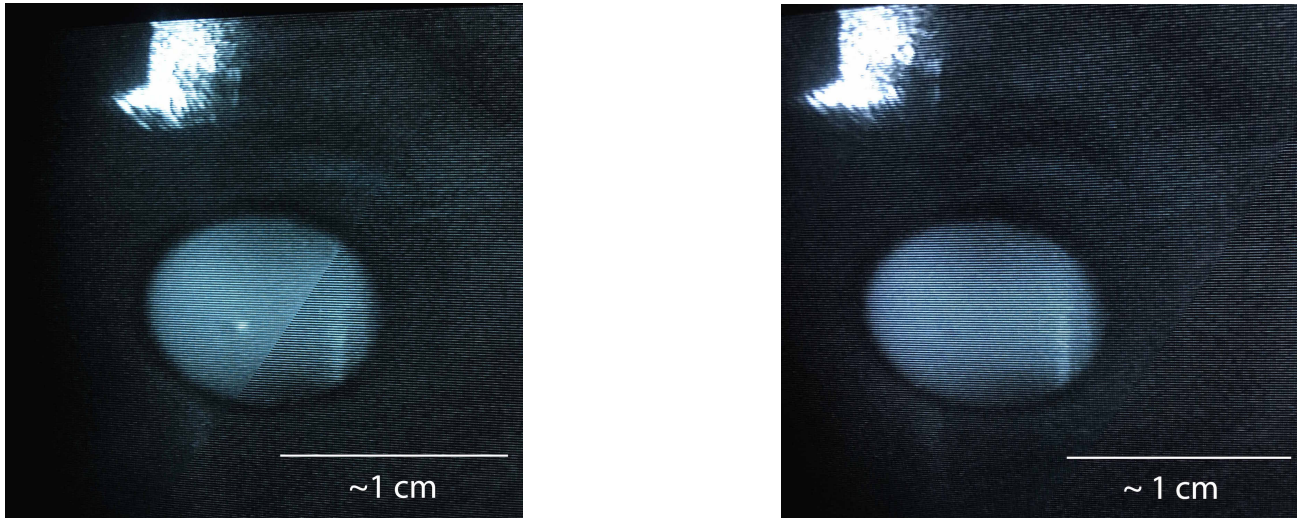

FIGURE 6.1. The image on the left was taken with a 2D MOT (the bright spot) present and the image on the right was taken in the absence of a 2D MOT. The view is looking up into lower vacuum chamber.

Shortly after seeing a 2D MOT progress was halted again while waiting for additional optomechanical parts to be machined. We received the rest of the parts with less than two weeks left before the deadline for this thesis, but were still hopeful there would be time to see a 3D MOT. We planned to characterize the loading rate, lifetime, and atom number of the MOT by measuring florescence with a photo diode. Unfortunately, in the true spirit of Murphy's law with one week remaining before the required submission of this document, the RuBECi vacuum system failed. We had 2D+ MOT up and running in the morning and had begun to look for a 3D MOT when poor alignment of the 3D MOT beams was observed. The getter was turned off to save rubidium while we made the appropriate adjustments. In the time it took to break for lunch and realign the 3D MOT beams the RuBECi vacuum had failed. We discovered the failure when we did not observe a 2D MOT, or any fluorescence in the lower vacuum chamber after turning the getter back on to resume the 3D MOT search. When examining the cell more closely we found what appeared to be a fish scale fracture, as shown in Figure 6.2, that might be the cause of the leak. We cannot be certain that this fracture is the cause of the problem because we do not have pictures of the cell from before the failure to confirm that the fracture was not present. It does, however, seem to be the likely cause.

There have been unconfirmed reports of similar failures of ColdQuanta RuBECi vacuum systems from the group working on the CAL project at the NASA Jet Propulsion Laboratory (JPL) [51]. This is does not bode well for the CAL project, because if the vacuum system in the apparatus being sent to the ISS fails the project will be seriously set back. In any case our RuBECi is being sent back to ColdQuanta for a proper diagnosis, and we will receive a new system. Sadly, this will not be in time for further results to be included in this thesis.

Once the new RuBECi arrives, the path forward for the experiment at Bates is pretty clear. After observing a 3D MOT the subsystems for optical pumping, radiofrequency evaporation, and absorption imaging need to be put in place. At this point we will be ready to load a MOT,
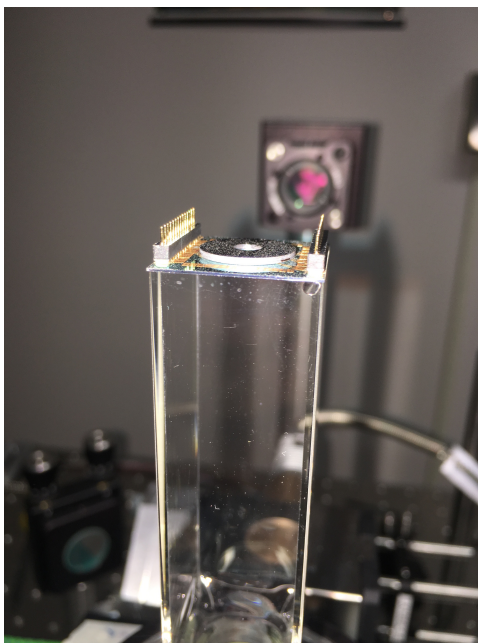
FIGURE 6.2. The crack we found in the upper chamber of the RuBECi, located in the upper right corner of the cell.

allow for sub-Doppler cooling in a brief optical molasses stage, optically pump the atoms into the $F = 2$, $M_F = 2$ state and load a quadrupole trap. From this point we can begin to work out the logistics of transferring the atoms to the atom chip. Once the atoms are loaded into a chip trap the final push towards condensation with evaporative cooling can be made. From this point on we should be able to make BECs and the question becomes what do with them. The first task for the new system is to use it as a testbed to aid in the development of experimental sequences for use in CAL, aboard the ISS. Afterwards there are any number of the possible research paths to pursue. No matter the choice the hope is that simplicity and ease of operation of the new experiment will make it accessible and user-friendly for generations of undergraduates to come.

References

[1] A. Einstein. Quantentheorie des einatomigen idealen gases. *Sitzungsber. Kgl. Preuss. Akad. Wiss.*, 261, 1924.

[2] A. Einstein. Quantentheorie des einatomigen idealen gases (zweite abhandlung). *Sitzungsber. Kgl. Preuss. Akad. Wiss.*, 3, 1925.

[3] M.R. Matthews C.E. Wieman E.A. Cornell M.H. Anderson, J.R. Ensher. Observation of bose-einstein condensation in a dilute atomic vapor. *Science*, 269:198.

[4] M. R. Andrews N. J. van Druten D. S. Durfee D. M. Kurn K.B. Davis, M.-O. Mewes and W. Ketterle. Bose-einstein condensation in a gas of sodium atoms. *Physical Review Letters*, 75:3969.

[5] J.J. Tollett C.C. Bradley, C. A. Sackett and R. G. Hulet. Evidence of bose-einstein condensation in an atomic gas with attractive interactions. *Physical Review Letters*, 269:1687.

[6] E. A. Cornell and C. E. Wieman. Nobel lecture: Bose-einstein condensation in a dilute gas, the first 70 years and some recent experiments. *Physical of Modern Physics*, 74:875.

[7] W. Ketterle. Nobel lecture: When atoms behave as waves: Bose-einstein condensation and the atom laser. *Physical of Modern Physics*, 74:1131.

[8] D.W. Snoke A. Griffin and S. Stringari. *Bose-Einstein Condensation*. Cambridge University Press, Cambridge, 1995.

[9] T. van Zoest et al. Bose-einstein condensation in microgravity. *Science*, 328:1540.

[10] David J. Griffits. *Introduction to Quantum Mechanics*. Pearson Education, Inc., NJ, 2005.

[11] Daniel V. Schroeder. *Thermal Physics*. Addison Wesley Longman, USA, 2000.

[12] R.K. Pathria. *Statistical Mechanics*. Pergamon Press, Canada, 1972.

[13] Massimo Inguscio and Leonardo Fallani. *Aromic Physics*. Oxford University Press, Oxford, 2013.

[14] C.J. Foot. *Atomic Physics*. Oxford University Press, Oxford, 2005.

[15] Ralph Baierlein. *Thermal Physics*. Cambridge University Press, Cambridge, 1999.

[16] Edward Moan. *Design and construction of multi-dimensional optical lattices for 87 Rb Bose-Einstein condensates*. PhD thesis, Bates College, 2014.

[17] James J. Kelly. Ideal quantum gases. Lecture Notes.

[18] Tom M. Apostol. *Introduction to Analytic Number Theory*. Springer-Verlag, NY, 1976.

[19] H. M. Edwards. *Riemann's Zeta Function*. Academic Press, NY, 1974.

[20] David E. Pritchard Vanderlei Bagnato and Daniel Kleppner. Bose-einstein condensation in an external potential. *Physical Review A*, 62:4354.

[21] Sandro Stringari Lev Pitaevskii. *Bose-Einstein Condensation*. Clarendon Press, Oxford, 2003.

[22] Peter van der Straten Harold J. Metcalf. *Laser Cooling and Trapping*. Springer-Verlag, NY, 1999.

[23] L. Allen. *Introduction to Analytic Number Theory*. John Wiley & sons, Inc., USA, 1975.

[24] Daniel A. Steck. Quantum and atom optics. 2015. available online at http://steck.us/alkalidata.

[25] Adriana Pálffy. *Spontaneous Emission: Weisskopf-Wigner Theory*. Lecture Notes.

[26] David J. Griffiths and J.H. Eberly. *Optical Resonance and Two-Level Atoms*. Pearson Education, Inc., IL, 2013.

[27] J.J. Sakurai. *Modern Quantum Mechanics*. The Benjamin/Cummings Publishing Company, Inc, California, 1985.

[28] Dieter Suter. *The Physics of Laser-Atom Interactions*. Cambridge University Press, Cambridge, 1977.

[29] Marc Tollin. Solving the optical bloch equations. *Bates College*, 2001.

[30] Steven Chu. Manipulation of neutral particles. *Review of Modern Physics*, 70:685.

[31] C.N. Cohen-Tannoudjii. Manipulating atoms with photons. *Review of Modern Physics*, 70:707.

[32] W.D. Phillips. Laser cooling and trapping of neutral atoms. *Review of Modern Physics*, 70:721.

[33] T.W. Hänsch and A.L. Schawlow. Cooling of gases by laser radiation. *Optics Communications*, 13:68.

[34] J. E. Bjorkholm Alex Cable Steven Chu, L. Hollberg and A. Ashkin. Three-dimensional viscous confinement and cooling of atoms by resonance radiation pressure. *Physical Review Letters*, 55:48.

[35] W.D. Phillips. Laser cooling and trapping of neutral atoms. *Office of Naval Research*, 1992.

[36] C. Cohen-Tannoudjii J. Dalibard. Sisyphus cooling of a bound atom. *Optical Society of America B*, 9:32.

[37] Alex Cable Steven Chu E.L. Raab, M.Prentiss and D.E Pritchard. Trapping of neutral sodium atoms with radiation pressure. *Physical Review Letters*, 59:2631.

[38] John V. Prodan and William D. Phillips. Chirping the lightfantastic? recent nbs atom cooling experiments. *Progress in Quantum Electronics*, 8:231.

[39] William D. Phillips and Harold Metcalf. Laser deceleration of an atomic beam. *Physical Review Letters*, 48:596.

[40] M. Weidemüller K. Dieckmann, R.J.C. Spreeuw and J.T.M. Walraven. Two-dimensional magneto-optical trap as a source of slow atoms. *Physical Review A*, 35:3891.

[41] R. Löw V. Schweikhard A. Grabowski Yu. B. Ovchinnikov J. Schoser, A. Batär and T. Pfau. Intense source of cold rb atoms from a pure two-dimensional magneto-optical trap. *Physical Review A*, 66:023410, 2002.

[42] Daniel A. Steck. Rubidium 87 d line data. 2008. available online at http://steck.us/alkalidata.

[43] Jörg Schmiedmayer Johannes Denschlag Ron Folman, Peter Krüger and Carsten Henkel. Microscopic atom optics: from wires to an atom chip. *Adv. in At. Mol. Opt. Physics*, 48:263.

[44] John V. Prodan Alan L. Migdall and William D. Phillips. First observation of magnetically trapped neutral atoms. *Physical Review Letters*, 54:2596.

[45] C.V. Sukumar and D.M. Brink.

[46] Immanuel Bloch Tilman Esslinger and Theodor W. Hänsch. Bose-einstein condensation in a quadrupole-ioffe-configuration trap. *Physical Review A*, 58:2664.

[47] T. W. Hänsch W. Hänsel, P. Hommelhoff and J. Reichel. Boseeinstein condensation on a microelectronic chip. *Nature*, 413:498.

[48] Grant R. Fowels. *Introduction to Modern Optics*. Holt, Rinehart, and Winston, NY, 1975.

[49] *Quadrupole Coil Assembly User Manual*. Cold Quanta, inc, Boulder, CO, 2013.

[50] Evan A. Salim Daniel M. Farkas and Jaime Ramirez-Serrano. Production of rubidium bose-einstein condensates at a 1 hz rate. *arXiv*, 2014.

[51] Nathan Lundblad. personal communication.